INFORMATION TO USERS

This manuscript has been reproduced from the microfilm master. UMI films the text directly from the original or copy submitted. Thus, some thesis and dissertation copies are in typewriter face, while others may be from any type of computer printer.

The quality of this reproduction is dependent upon the quality of the copy submitted. Broken or indistinct print, colored or poor quality illustrations and photographs, print bleedthrough, substandard margins, and improper alignment can adversely affect reproduction.

In the unlikely event that the author did not send UMI a complete manuscript and there are missing pages, these will be noted. Also, if unauthorized copyright material had to be removed, a note will indicate the deletion.

Oversize materials (e.g., maps, drawings, charts) are reproduced by sectioning the original, beginning at the upper left-hand corner and continuing from left to right in equal sections with small overlaps.

ProQuest Information and Learning
300 North Zeeb Road, Ann Arbor, MI 48106-1346 USA
800-521-0600

Simulation of Reactive Components by the TLM Method

by
Yuan Yue

A thesis submitted to the
School of Graduate Studies and Research
in partial fulfillment of the requirements for the degree of

Master of Applied Science

Ottawa-Carleton Institute for Electrical Engineering

Department of Electrical Engineering
Faculty of Engineering
University of Ottawa

I hereby declare that I am the sole author of this thesis. I authorize the University of Ottawa to lend this thesis to other institutions or individuals for the purpose of shcolarly research.

Yuan Yue

I further authorize the University of Ottawa to reproduce this thesis by photocopying or by other means, in total or in part, at the request of other institutions or individuals for the purpose of scholarly research.

Yuan Yue

Contents

Abstract

Several new models for the simulation of nonlinear components have been developed in this thesis.

Firstly, the model of the stub terminated with a constant capacitance is established. Simulations of a lumped capacitance connected to a transmission line, as well as modelling of relative permittivity can be done by this approach.

Secondly, the algorithm for the modelling of voltage-dependent capacitance is developed based on the model of the stub terminated with variable capacitance.

Thirdly, a configuration for the simulation of series capacitance in the TLM mesh is derived. The scattering matrix and the transmission formula for the structure are developed. The structure can also be used to simulate series-connected varactor diodes.

Finally, the simulation of a varactor diode is performed in the three-dimensional expanded-node scheme.

In order to show the application of different models, some examples, simulation results and discussions are given in this thesis.

Acknowledgements

I would like to thank my supervisors Dr W. J. R. Hoefer and M. Ney for their help, encouragement and financial support over the course of my graduate studies. I would like to particularly thank them for their many useful comments concerning the research and the writing of the thesis.

Dr Harrison's helpful suggestions and valuable information are also acknowledged.

The author expresses her gratitude to her colleagues for the valuable discussions we had.

List of Figures

List of Tables

List of Symbols

c	Velocity of light in free space
μ_0	Permeability of free space
ϵ_0	Permittivity of free space
η_0	Intrinsic impedance of free space
μ_r	Relative permeability of a medium
ϵ_r	Relative permittivity of a medium
C	Capacitance per unit length for transmission line
L	Inductance per unit length for transmission line
C_l	Loading capacitance on the end of stubs
R_l	Loading resistance on the end of stubs
y_0	Normalized characteristic admittance of the open-circuited stub
y_r	Normalized characteristic admittance of the stub loaded with lumped element
Y_0	Characteristic admittance of a TLM mesh line
Y_r	Characteristic admittance of a stub
Z_t	Characteristic impedance of a transmission line
Y_t	Characteristic admittance of a transmission line
Z_0	Intrinsic impedance of free space
$\mathcal{F}$	Function of discrete Fourier transform
α	Equivalent attentuation constant of the mesh transmission line
β	Equivalent phase constant of the mesh transmission line
α_n	Attentuation constant of a wave on TLM mesh along a main axis
β_n	Phase constant of a wave on TLM mesh along a main axis
λ	Wave length of electromagnetic wave

$h[n]$	Impulse response of a discrete linear system

Chapter 1

Introduction

1.1 Motivation

After the varactor diode was developed in the middle of the 1950's in Bell Telephone Laboratories, Inc.[18], it soon became a very important product in microwave industry. It has been widely used in low-noise microwave parametric amplifiers, in low-noise small-signal frequency converters and in frequency mutipliers, dividers and mixers. Also, it has been employed in voltage-controlled oscillators for modulators.

Most of the analyses of the varactor application have been done in the frequency domain and were based on the lumped equivalent circuit of the varactor diode. And usually, the analysis results which are given as performance limits are obtained for the varactor diode itself. However, unless the effects of the embedding circuit is included, these analyses are certainly not accurate and convenient for modern microwave circuit design. Especially for the case of microwave and millimeter-wave monolithic integrated circuits, it is very difficult and almost impossible to adjust the characteristics once the circuits are fabricated. Therefore, an accurate and flexible analysis method which can account for both the diode and the embedding circuits is needed for the design of different circuits involving the nonlinear elements.

Fortunately, the newly developed transmission line matrix (TLM) method is very suitable for the simulation of microwave circuits because of its flexibility and high accuracy. It has been successfully used for the extraction of scattering parameters, resonant frequencies and dispersion characteristics of microwave components. As a time domain numerical method, the TLM method also provides the possibility to analyze nonlinear devices in the

time domain. Thus, to model the equivalent circuit of such elements by TLM will hopefully make the analysis of nonlinear circuits easier and more accurate. Some work has been done by Kosmopoulos et al. [14]. Based on these previous results and new developments in TLM simulation, a new model for the TLM implementation of lumped constant capacitance and of varactor diodes has been studied in this thesis. A model for the series-connected varactor diode is developed as well, and the simulation of varactor diodes is extended to three dimensions.

1.2 Introduction to the TLM method

Back in 1944, an equivalent circuit had been developed by Kron[15] representing the field equations of Maxwell. In the same year, Whinnery and Ramo [21] sucessfully applied this equivalent circuit to the solution of high-frequency field problems using a two-dimensional Cartesian mesh. Inspired by the above ideas, Johns and Beurle first developed the transmission line matrix method , by which very good results were obtained for two-dimensional scattering problems in 1971. Subsequent papers by Johns and Akhtarzad applied this method to inhomogeneous [13] and lossy [3] problems and also extended this method to three-dimensional cases[4]. Various features and improvements were also added by other researchers in a short period of time. Now the TLM method has become a very powerful time domain numerical method for the simulation of microwave and millimeter-wave structures.

1.2.1 The TLM Mesh and the Equivalence between the Wave Equations and Maxwell's Equations

In the two-dimensional case, the space is represented by a Cartesian transmission line mesh which has the mesh parameter of Δl (see Figure 1.1). The nodes represent the junctions between the transmission lines. Depending on the different type of connections, there are two kinds of nodes - shunt node and series node (see Figure 1.2). The unit time Δt is the time required for an electromagnetic impulse to travel from one node to the next. In this way, the space and the time have been discretized by Δl and Δt, respectively.

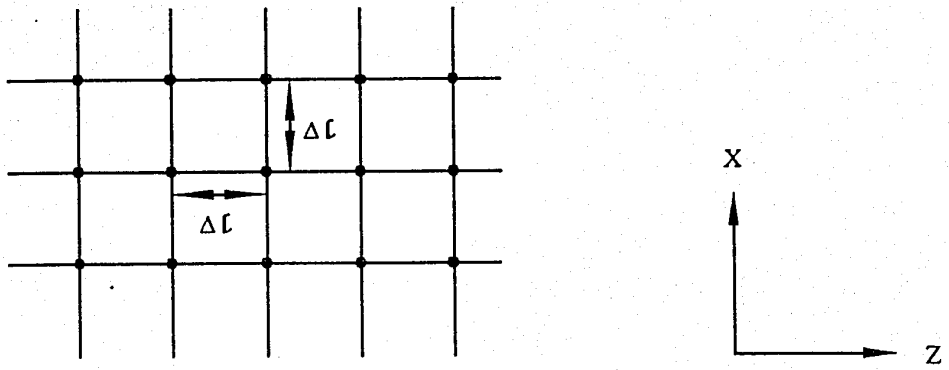

Fig. 1.1: The transmission line matrix mesh in two dimensions

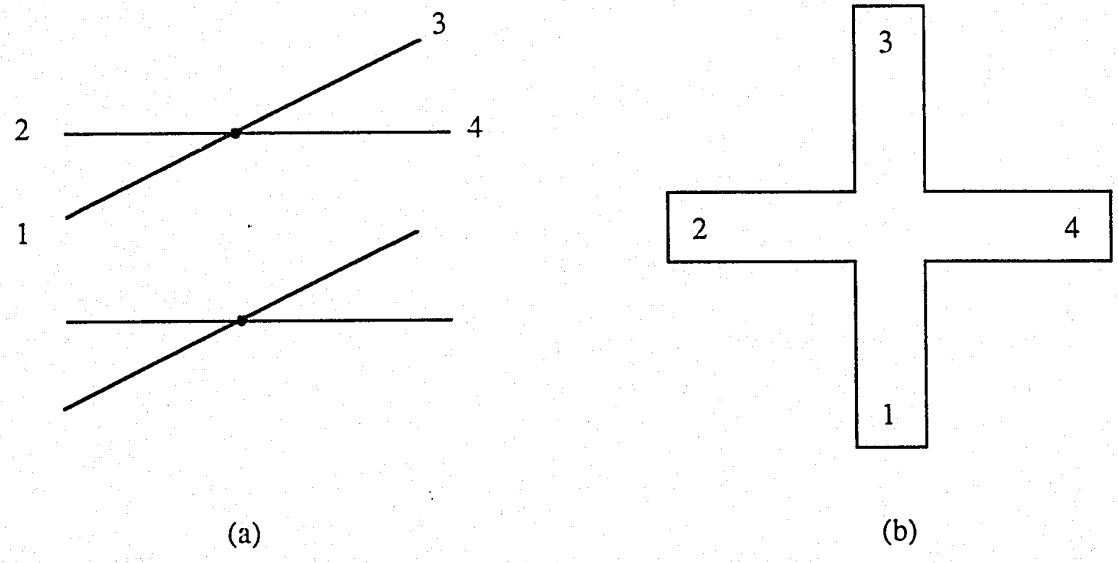

Fig. 1.2: a) shunt node b) series node

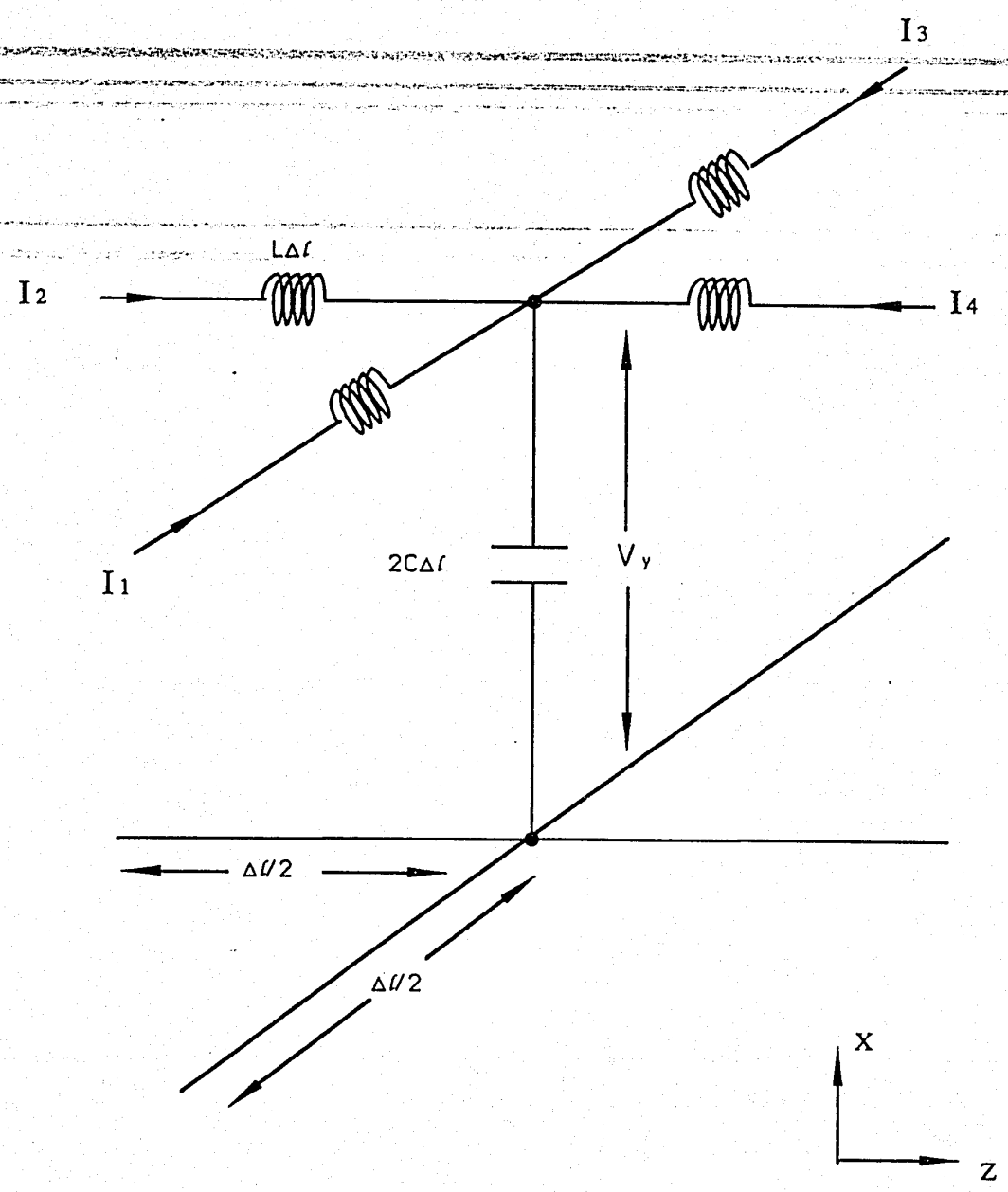

Fig. 1.3: The equivalent circuit of the shunt node

Taking a simple shunt-connected TLM mesh as an example, the equivalence between the voltages and currents on the line mesh and the electric and magnetic fields solutions of Maxwell's equations will be presented clearly.

Assuming that the mesh is fine enough, i.e. $\Delta l << \lambda$, the transmission line can be approximated by the lumped circuit shown in figure 1.3. L and C are the inductance and capacitance per unit length of an individual transmission line. The voltage and currents in the mesh are related by:

$$\frac{\partial V_y}{\partial x} = -L\frac{\partial (I_1 - I_3)}{\partial t} \tag{1.1}$$

$$\frac{\partial V_y}{\partial z} = -L\frac{\partial (I_2 - I_4)}{\partial t} \tag{1.2}$$

$$\frac{\partial (I_1 - I_3)}{\partial z} + \frac{\partial (I_2 - I_4)}{\partial x} = -2C\frac{\partial V_y}{\partial t} \tag{1.3}$$

Combining equations (1.1) to (1.3), yields the wave equation:

$$\frac{\partial^2 V_y}{\partial x^2} + \frac{\partial^2 V_y}{\partial z^2} = 2LC\frac{\partial^2 V_y}{\partial t^2} \tag{1.4}$$

Equations (1.5) to (1.7) are expansions of Maxwell's equations for $\frac{\partial}{\partial y} = 0$, and $E_x = E_z = H_y = 0$ (which is the condition for the TE_{n0} mode in a rectangular waveguide. z is the longitudinal direction). Equation (1.8) is obtained by combining the equations (1.5) to (1.7).

$$\frac{\partial E_y}{\partial z} = \mu\frac{\partial H_x}{\partial t} \tag{1.5}$$

$$\frac{\partial E_y}{\partial x} = -\mu\frac{\partial H_z}{\partial t} \tag{1.6}$$

$$\frac{\partial H_x}{\partial z} - \frac{\partial H_z}{\partial x} = -\epsilon\frac{\partial E_y}{\partial t} \tag{1.7}$$

and

$$\frac{\partial^2 E_y}{\partial x^2} + \frac{\partial^2 E_y}{\partial z^2} = \mu\epsilon\frac{\partial^2 E_y}{\partial t^2} \tag{1.8}$$

Comparing equation (1.4) with equation (1.8), it is easy to find the equivalence below:

$$
\begin{aligned}
E_y &\equiv V_y \\
h_z &\equiv I_x \\
\mu &\equiv L \\
\epsilon &\equiv 2C \quad .
\end{aligned} \tag{1.9}
$$

This equivalence makes it possible to get the solution for field problems by studying the voltages and currents in the TLM mesh. The only condition is that Δl should be small enough(about 1/10 of a wavelength or less). The dispersion of the velocity of the wave on the two-dimensional TLM network is also discussed in [5]. If the impulses travel at the speed of light on each transmission line linking the neighbouring nodes, i.e.

$$
\frac{1}{\sqrt{LC}} \equiv \frac{1}{\sqrt{\mu_0 \epsilon_0}} = c \quad , \tag{1.10}
$$

then equation (1.4) leads to the conclusion that the velocity of the wave on the mesh is:

$$
\frac{1}{\sqrt{2LC}} = \frac{c}{\sqrt{2}} \quad . \tag{1.11}
$$

This means that the wave propagation velocity in the TLM mesh is $\frac{1}{\sqrt{2}}$ times the velocity of light when the impulses travel on the mesh lines at the speed of light. In fact, the velocity of a wave on the TLM mesh is always $\frac{1}{\sqrt{2}}$ times less than that of the impulses travelling on the mesh lines. At the same time, the impedance of the mesh line is $\frac{1}{\sqrt{2}}$ times smaller than that of the medium which is represented by the TLM mesh. This factor should always be considered carefully in any transformations between the TLM mesh and real circuits.

1.2.2 Scattering and Transmission on the TLM Mesh

Taking the general shunt node as an example, a brief description of scattering and transmission is given here. The general shunt node has been developed by Akhtarzad [12] for the simulation of lossy inhomogeneous media. Based on the simple shunt node, a permittivity stub and a loss stub (or a lumped normalized shunt conductance g_0) are added to the node (see Figure 1.4). The permittivity stub is an open-circuited transmission line of length $\frac{\Delta l}{2}$

and normalized characteristic admittance y_0. The loss stub is a matched transmission line of normalized characteristic admittance g_0.

Comparing the wave equations of the mesh made of general shunt nodes with Maxwell's equations for a medium having a complex permittivity ($\epsilon = \epsilon_0\epsilon_r + \frac{\sigma}{j\omega}$), two more equivalences are obtained in addition to equation (1.9) :

$$\sigma \equiv \frac{g_0 Cc}{\Delta l}$$
$$\epsilon_r \equiv 1 + \frac{y_0}{4} \qquad (1.12)$$

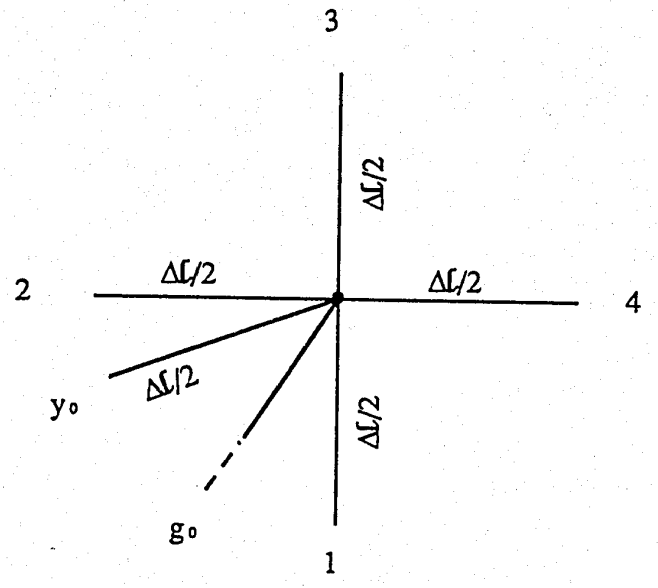

Fig. 1.4: Shunt node with permittivity and loss stubs

The scattering matrix for the node then becomes:

$$
{}_k\begin{bmatrix} V_1 \\ V_2 \\ V_3 \\ V_4 \\ V_5 \end{bmatrix}^r = \frac{1}{y}\begin{bmatrix} -(y-2) & 2 & 2 & 2 & 2y_0 \\ 2 & -(y-2) & 2 & 2 & 2y_0 \\ 2 & 2 & -(y-2) & 2 & 2y_0 \\ 2 & 2 & 2 & -(y-2) & 2y_0 \\ 2 & 2 & 2 & 2 & 2y_0 - y \end{bmatrix} {}_k\begin{bmatrix} V_1 \\ V_2 \\ V_3 \\ V_4 \\ V_5 \end{bmatrix}^i
$$

where

$$
\begin{aligned}
y &= 4 + y_0 + g_0 && (1.13)\\
y_0 &= 4(\epsilon_r - 1) && (1.14)\\
g_0 &= \frac{\sigma \triangle l}{Cc} \ . && (1.15)
\end{aligned}
$$

After scattering, the impulses reflected from the nodes will become the incident impulses on the neighbouring nodes. The transmission on the mesh can be implemented by:

$$
\begin{aligned}
{}_{k+1}V_1^i(z,x) &= {}_kV_3^r(z,x-1)\\
{}_{k+1}V_2^i(z,x) &= {}_kV_4^r(z-1,x)\\
{}_{k+1}V_3^i(z,x) &= {}_kV_1^r(z,x+1)\\
{}_{k+1}V_4^i(z,x) &= {}_kV_2^r(z+1,x)\\
{}_{k+1}V_5^i(z,x) &= {}_kV_5^r(z,x)
\end{aligned}
$$

Through repetitive iteration of scattering and transmission, the time domain responses of the electromagnetic fields can be obtained as:

$$
\begin{aligned}
{}_kE_y \equiv {}_kV_y &= \frac{2}{y}\Big(\sum_{m=1}^{4} {}_kV_m^i + {}_k V_5^i y_0\Big)\\
-{}_kH_x \equiv {}_kI_z &= \frac{{}_kV_2^i - {}_k V_4^i}{Z_0}\\
{}_kH_z \equiv {}_kI_x &= \frac{{}_kV_1^i - {}_kV_3^i}{Z_0} && (1.16)
\end{aligned}
$$

The frequency domain response can be obtained by taking the discrete Fourier transform of the time domain output stream ($_kA$). A could be any one of the field components listed above.

$$Re[\mathcal{F}(\frac{\Delta l}{\lambda})] = \sum_{k=1}^{N} {}_kA\cos(2\pi k\frac{\Delta l}{\lambda}) \tag{1.17}$$

$$Im[\mathcal{F}(\frac{\Delta l}{\lambda})] = -\sum_{k=1}^{N} {}_kA\sin(2\pi k\frac{\Delta l}{\lambda}) \tag{1.18}$$

The accurate range of results is limited by the dispersive characteristics of the mesh.

1.2.3 Dispersion Characteristics of the 2D-TLM mesh

The frequency-dependent propagation constant of TEM waves in the stub-loaded mesh is derived in [1]. If the complex propagation constant on the individual mesh line is

$$\gamma = \alpha + j\beta \tag{1.19}$$

the complex propagation constant of a TEM wave in the TLM mesh is

$$\gamma_n = \alpha_n + j\beta_n \quad . \tag{1.20}$$

As shown in figure 1.5, the phase constant β_n and attenuation constant α_n of the wave on the TLM mesh are functions of the normalized frequency for various values of the normalized characteristic admittance y_0. α and β represent equivalent propagation characteristics of the mesh transmission lines. At relatively low frequency ($\frac{\Delta l}{\lambda} \ll 1$) when the dispersion is small, and we have:

$$\gamma_n = \sqrt{2(1+\frac{y_0}{4})}\gamma \tag{1.21}$$

With increasing y_0, the dispersion becomes stronger and the useful frequency range is reduced.

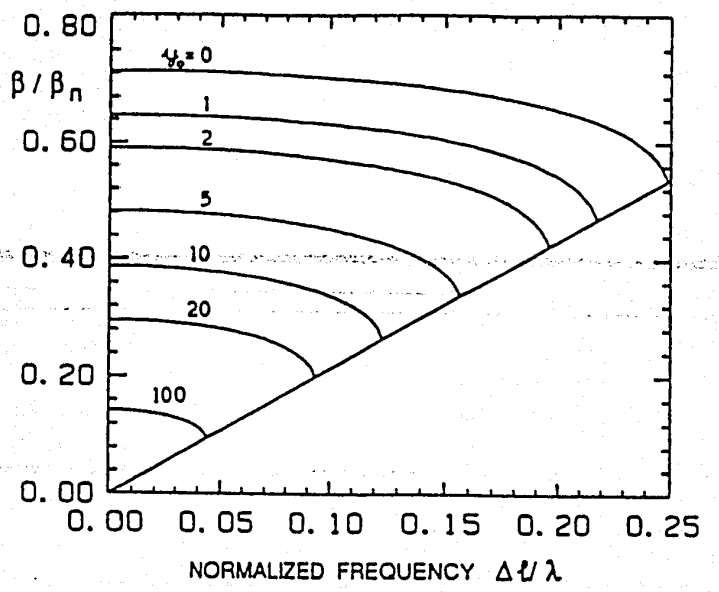

(a)

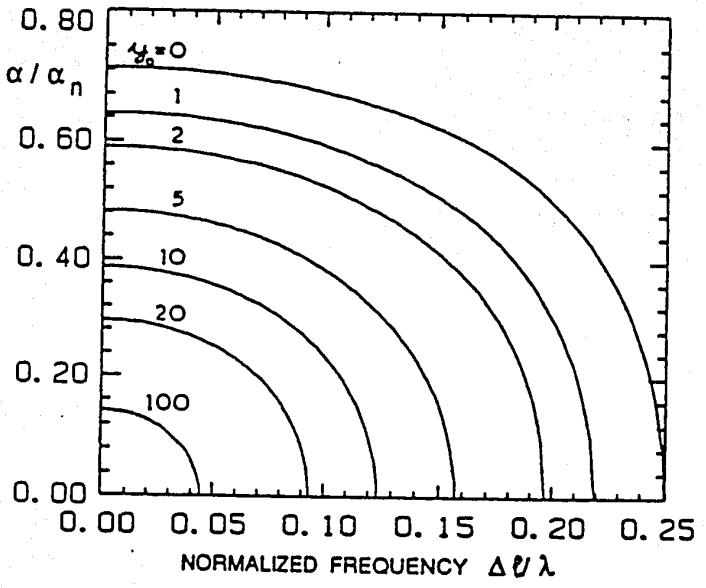

(b)

Fig.1.5 (a) Attenuation characteristic for plane TEM waves travelling along a main axis in a two-dimensional stub-loaded shunt TLM network.

(b) Phase characteristic for plane TEM waves travelling along a main axis in a two-dimensional stub-loaded shunt TLM network.(After Aktharzad [1]).

1.2.4 Excitation of the TLM Mesh

The TLM mesh can be excited simply by inserting one or several impulses at one, or more than one node. Impulse excitation is suitable for computing the impulse response of a structure. To simulate a continuous wave, a stream of impulses which has the same envelope as that of the continuous wave should be added at each iteration to the impulses already present in the mesh. A calibrated voltage source can be modelled in the form of Huygens sources backed by an absorbing wall [20] as shown in figure 1.6.

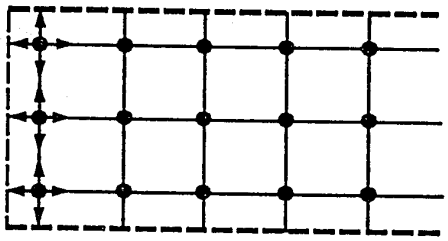

Fig. 1.6: Modelling of a matched voltage source in a parallel-plate waveguide with magnetic sidewalls.

Absorbing wall

Magnetic wall

Assuming that the electric field amplitude of the input TEM travelling wave at the excitation points is represented by V^+ in the TLM mesh, and that the effective permittivity of the medium is ϵ_{eff}, then the magnitude of the voltage impulses launched from each source point into its four main branches should be

$$V_k^r = \sqrt{\frac{\epsilon_{eff}}{2}} V^+ \quad . \tag{1.22}$$

1.3 Conclusion

In this chapter, a brief summary of the 2D-TLM algorithm and the characteristics of the 2D-TLM shunt mesh has been presented. The knowledge of these basic concepts is employed in the further developments presented in the following chapters.

Chapter 2

Properties of Shunt Stubs Loaded with Constant Capacitance

2.1 Introduction

This chapter introduces the stub loaded with constant capacitance, which can be used to simulate both lumped capacitance and distributed relative permittivity.

2.2 Stub Model Loaded with Constant Capacitance

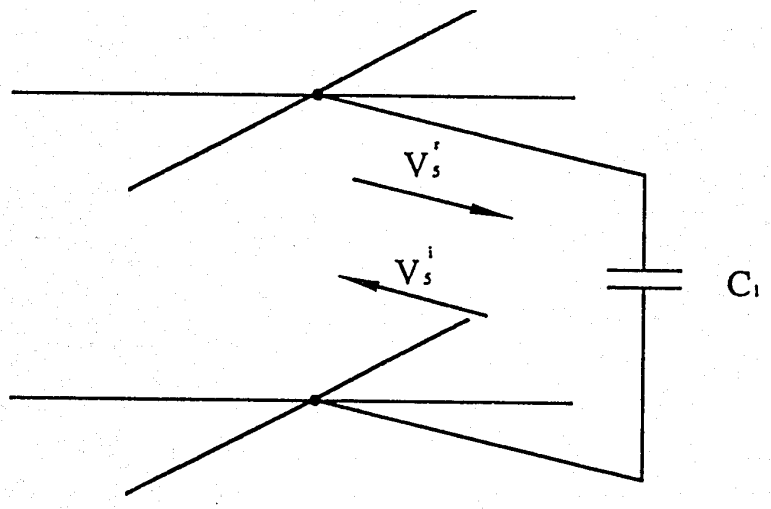

Fig. 2.1 : TLM shunt node with lumped capacitance

The open-circuited stub of length $\Delta l/2$ has been sucessfully used to model a medium with an arbitrary relative permittivity [5]. The values of ε_r is determined by the choice of the characteristic admittance of the open-circuited stub. However, in the present work, the length and the characteristic admittance of stubs are kept constant, but the stub itself is terminated by a lumped capacitance (C_l) as shown in figure 2.1. The impulses V_5^i reflected by this capacitance are obtained by stepwise integrating the differential equation governing the voltage-current relationship of the capacitance, as will be discussed below.

Generally, the real normalized characteristic admittance of the stub y_r may be chosen arbitrarily. Here, we choose $y_r = 4.0$, in order to match the stub to the node. The scattering matrix for the TLM shunt node comprising a stub of $y_r = 4$ becomes [19]:

$$
{}_k\begin{bmatrix} V_1 \\ V_2 \\ V_3 \\ V_4 \\ V_5 \end{bmatrix}^r
=
\begin{bmatrix}
-\frac{3}{4} & \frac{1}{4} & \frac{1}{4} & \frac{1}{4} & 1 \\
\frac{1}{4} & -\frac{3}{4} & \frac{1}{4} & \frac{1}{4} & 1 \\
\frac{1}{4} & \frac{1}{4} & -\frac{3}{4} & \frac{1}{4} & 1 \\
\frac{1}{4} & \frac{1}{4} & \frac{1}{4} & -\frac{3}{4} & 1 \\
\frac{1}{4} & \frac{1}{4} & \frac{1}{4} & \frac{1}{4} & 0
\end{bmatrix}
\cdot
{}_k\begin{bmatrix} V_1 \\ V_2 \\ V_3 \\ V_4 \\ V_5 \end{bmatrix}^i
$$

As shown in the scattering matrix above, since the stub is matched to the node, the voltage impulse ${}_kV_5^r$ depends only on the voltage impulses ${}_kV_1^i$ to ${}_kV_4^i$ and not on the voltage impulse ${}_kV_5^i$ incident from the stub. Therefore, ${}_kV_5^r$ may be computed directly from the voltage impulses incident on the link lines without solving a nonlinear equation.

Referring to figure 2.2, the stub is connected to the TLM shunt node at $B - B$. It will take an interval $\Delta t/2$ ($\Delta t = \frac{\Delta l}{c}$) for the voltage impulse ${}_kV_5^r$ to travel from the node to the lumped capacitance. At this point, the voltage on the capacitance will be the sum of ${}_kV_5^r$ and ${}_kV_5^i$. After another time interval of $\Delta t/2$, the voltage impulse ${}_kV_5^i$ coming from the stub will reach the node at the same time as the voltage impulses being reflected from the other branches. So the synchronism of impulses on the entire TLM mesh is ensured.

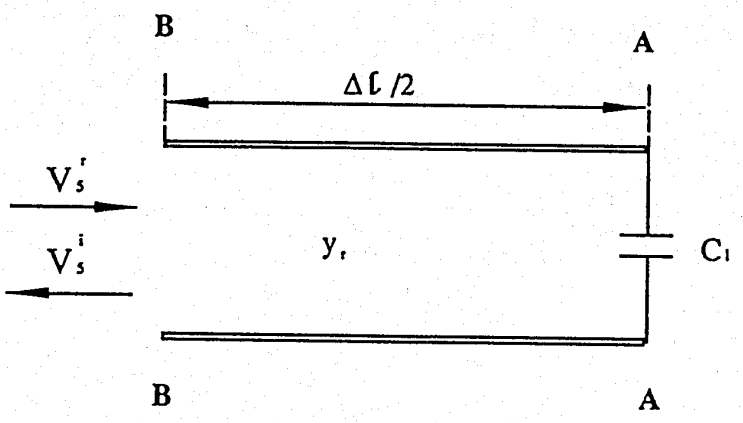

Fig. 2.2: The stub terminated with constant capacitance

At $A-A$, we have

$$v(t) = v_5^r(t) + v_5^i(t) \tag{2.1}$$

$$i(t) = Y_r[v_5^r(t) - v_5^i(t)] \tag{2.2}$$

$$\frac{dv_{(t)}}{dt} = \frac{i(t)}{C_l} \quad . \tag{2.3}$$

Y_r is the real characteristic admittance of the stub. Because we assume $y_r = 4.0$, Y_r will be four times the characteristic admittance of the link lines of the TLM mesh.

Discretizing equations (2.1) to (2.3) yields

$${}_kV = {}_kV_5^r + {}_k V_5^i \tag{2.4}$$

$${}_kI = Y_r[{}_kV_5^r - {}_k V_5^i] \tag{2.5}$$

$${}_{k+1}V - {}_k V = \frac{{}_{k+1}I}{C_l}\Delta t \tag{2.6}$$

thus

$${}_{k+1}V_5^i = \frac{{}_kV_5^r + {}_k V_5^i}{1 + \frac{Y_r}{C_l}\Delta t} + \frac{\frac{Y_r}{C_l}\Delta t - 1}{1 + \frac{Y_r}{C_l}\Delta t}\ {}_{k+1}V_5^r \quad . \tag{2.7}$$

In equation (2.6), we have the option to choose the ${}_{k+1}I$ or ${}_{k}I$ corresponding to the forward and backward difference. It will be shown in the next chapter that the model has better stability if the forward difference is used. By using ${}_{k}I$ instead of ${}_{k+1}I$ in equation (2.6), we have

$$ {}_{k+1}V_5^i = -{}_{k+1}V_5^r + {}_{k}V_5^r(1 + \frac{Y_r \Delta t}{C_l}) + {}_{k}V_5^i(1 - \frac{Y_r \Delta t}{C_l}) \tag{2.8} $$

In both equations (2.7) and (2.8), the incident voltage impulse ${}_{k+1}V_5^i$ depends not only on the reflected voltage impulse ${}_{k+1}V_5^r$, but also on the incident and reflected voltage impulses at the previous iteration. This is due to the reactance characteristics of the capacitance. In simulation, both formulas give identical results. provided that the time step is sufficiently small and the stability conditions are satisfied. The stabilitity for these two formulas will be discussed later in this chapter.

2.3 Application of the Stub Model Loaded with Capacitance

2.3.1 Simulation of a Lumped Capacitance

Figure 2.3 (a) shows a transmission line resonator which is open-circuited at both ends. On the right side. a lumped capacitance C_n is added $\frac{\Delta l}{2}$ away from the end. The corresponding TLM mesh for the resonator is shown in figure 2.3 (b). Since the relative permittivity of the transmission line is 2, every node in TLM mesh comprises a open-circuited stub of $y_r = 4$. To simulate the lumped capacitance C_n, the stub of the node right in front of the magnetic wall is loaded with a capacitance C_l. C_l is related to C_n by:

$$ C_l = 2C_n \tag{2.9} $$

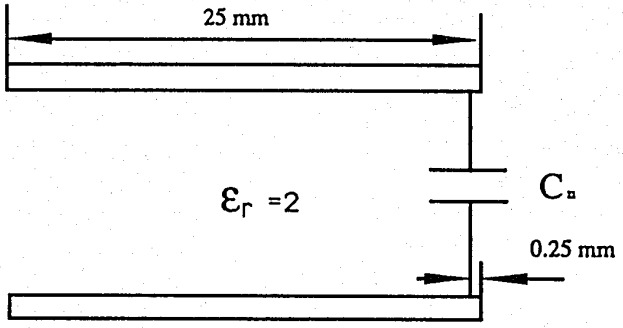

(a)

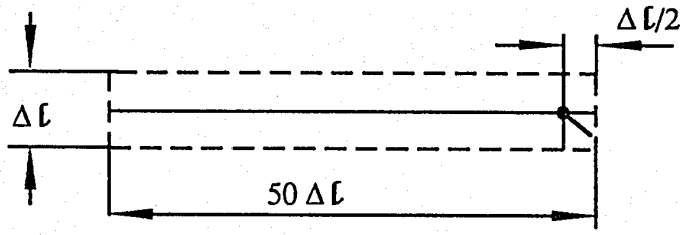

(b)

Fig. 2.3 : (a) The transmission line resonator with a lumped capacitance C_n

(b) The TLM mesh for (a) with Δl =0.5 mm, C_1 terminate the stub of the node at the right end.

– – – – – – – Magnetic wall

This is due to the factor of $\frac{1}{\sqrt{2}}$ in the transformations of frequency and impedance between the TLM mesh and the real case it simulates. These have been discussed in chapter 1. For cases where the transmission line has an arbitary relative permittivity, equation (2.9) should be replaced by equation (2.23) which is discussed later in section 2.3.3. Since the characteristic admittance of the stub has been set to four times the characteristic admittance of the mesh lines, we have

$$Y_r = 4\sqrt{\frac{C}{L}} = \frac{4}{\eta_0} \quad . \tag{2.10}$$

For different values of capacitance (C_l) at the end of the stubs in the submesh, the corresponding first resonant frequencies (f_0) can be obtained from the TLM simulation, followed by Fourier transformation.

Using steady-state transmission line theory, we can also get the theoretical values of the first resonant frequency f_a for the structure shown in figure 2.3 (a). f_a must satisfy the equation

$$Y_t[\tan(\frac{2\pi f_a l_2}{v}) - \cot(\frac{2\pi f_a l_1}{v})] + 2\pi f_a C_n = 0 \tag{2.11}$$

where

$$\begin{aligned} v &= \frac{c}{\sqrt{\epsilon_r}} \\ Y_t &= \frac{\sqrt{\epsilon_r}}{\eta_0} \\ l_1 &= 49.5 \triangle l \\ l_2 &= 0.5 \triangle l \\ \triangle l &= 0.5mm \quad . \end{aligned}$$

By solving the transcendental equation (2.11), the analytical solution of f_0 can be obtained for different lumped capacitance values C_n.

Comparing the simulation results f_0 with the analytical value f_a in table 2.1, the errors are acceptable.

C_a (pF)	C_1 (pF)	f_0 (GHz)	f_a (GHz)	Error = $\frac{\lvert f_a - f_0 \rvert}{f_a}$ (%)
0.1	0.2	1.72	1.739	1.1
0.2	0.4	1.50	1.496	0.27
0.4	0.8	1.18	1.207	2.2
0.6	1.2	1.02	1.038	1.8
1.2	2.4	0.77	0.7756	0.7
1.6	3.2	0.67	0.6816	1.7
2.0	4.0	0.61	0.6151	0.8
2.5	5.0	0.53	0.5542	4.4
3.0	6.0	0.502	0.5083	1.2
3.5	7.0	0.464	0.4723	1.8

Table 2.1 : The simulation and analytical results for the first resonant frequency of the resonator in Fig. 2.3. f_0 is obtained from TLM simulation. f_a is obtained by solving equation (2.11).

2.3.2 Simulation of a Relative Permittivity

The relative dielectric constants of the TLM subregions can be modeled in two different ways. The first approach, which was proposed by Johns [13], consists of adding open-circuited stubs to the shunt nodes. The stubs have a length of $\frac{\Delta l}{2}$ and a characteristic admittance of Y_r. The normalized characteristic admittance is $y_0 = \frac{Y_r}{Y_0}$, where Y_0 is the characteristic admittance of the link lines of the TLM mesh. The relative permittivity which is simulated by the open-circuited stubs is:

$$\epsilon_r = 1 + \frac{y_0}{4} \quad . \tag{2.12}$$

The second approach, just derived in the previous section, consists of loading the sub-mesh with $\frac{\Delta l}{2}$ stubs of fixed characteristic admittance $y_r = 4$ and adding lumped capacitances C_l at the other end of the stubs. This, of course, allows us to model only relative permittivity larger than 2, because the stub alone (without the additional capacitance loading) already models an ϵ_r value of:

$$\epsilon_{rmin} = 1 + \frac{y_r}{4} = 2 \tag{2.13}$$

Additional capacitance C_l at the end of the stub will then increase ϵ_r above this value. If we assume that $\frac{\Delta l}{2}$ is very small compared to the wavelength, we can simply add the load capacitance to the capacitance already present at the shunt node. The total capacitance at each shunt node C_{node} will include three terms as below. The first two terms are the capacitance of the TLM mesh lines and the capacitance of the stub, respectively.

$$\begin{aligned} C_{node} &= 2C\,\Delta\,l + Cy_r\frac{\Delta l}{2} + C_l \\ &= 2C\,\Delta\,l[1 + \frac{y_r}{4} + \frac{C_l}{2C\,\Delta\,l}] \end{aligned} \tag{2.14}$$

As presented in section 1.2.2, if the relative permittivity is simulated by open-circuited stubs, the total capacitance added to every shunt node is:

$$\begin{aligned} C_{node} &= 2C\,\Delta\,l + Cy_0\frac{\Delta l}{2} \\ &= 2C\epsilon_r\,\Delta\,l \end{aligned} \tag{2.15}$$

Comparing equation(2.14) with (2.15), we can obtain:

$$2C\epsilon_r \triangle l = 2C \triangle l[1 + \frac{y_r}{4} + \frac{C_l}{2C \triangle l}] \quad . \tag{2.16}$$

Since y_r has been chosen as 4, this yields

$$\epsilon_r = 2 + \frac{C_l}{2C \triangle l} \quad , \tag{2.17}$$

resulting in

$$C_l = 2(\epsilon_r - 2)C \triangle l \quad . \tag{2.18}$$

For elementary transmission lines in the TLM mesh, the inductance and capacitance per unit length are related by:

$$\frac{1}{\sqrt{LC}} = \frac{1}{\sqrt{\epsilon_0 \mu_0}} \tag{2.19}$$

$$\sqrt{\frac{L}{C}} = \sqrt{\frac{\mu_0}{\epsilon_0}} \quad , \tag{2.20}$$

From the above two equations, it is easy to get

$$C = \epsilon_0 \quad . \tag{2.21}$$

Then finally we have:

$$C_l = 2\epsilon_0(\epsilon_r - 2) \triangle l \quad . \tag{2.22}$$

In order to simulate a relative permittivity ϵ_r, the stubs should be terminated with C_l which is given by equation (2.22).

Here, a simple inhomogeneous waveguide resonator problem is used to test the simulation of relative permittivity by the new model (see figure 2.4 (a)).

Simulation is done first by modelling the right section by open-circuited stubs with their normalized characteristic admittance y_0 determined according to equation (2.12), then by modelling the right section by capacitance-loaded stubs having $y_r = 4$ and C_l given by equation (2.22). The mesh shown in figure 2.4(b) is excited by an impulse. The first resonant frequencies obtained are listed in Table 2.2. Comparing the simulation results of the two methods, it is found that they both lead to similar resonant frequency values. Comparing the simulation results with the analytical solutions, the errors are typically of the order of one percent.

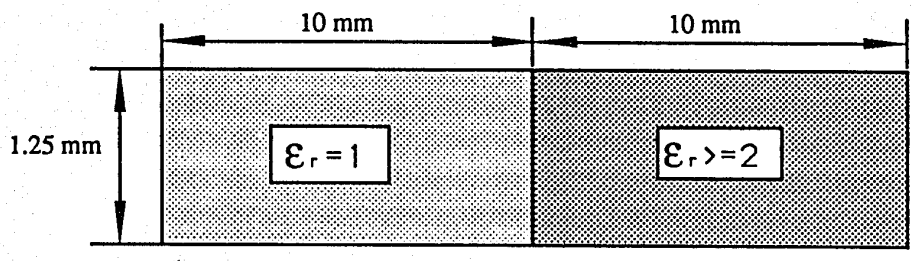

(a)

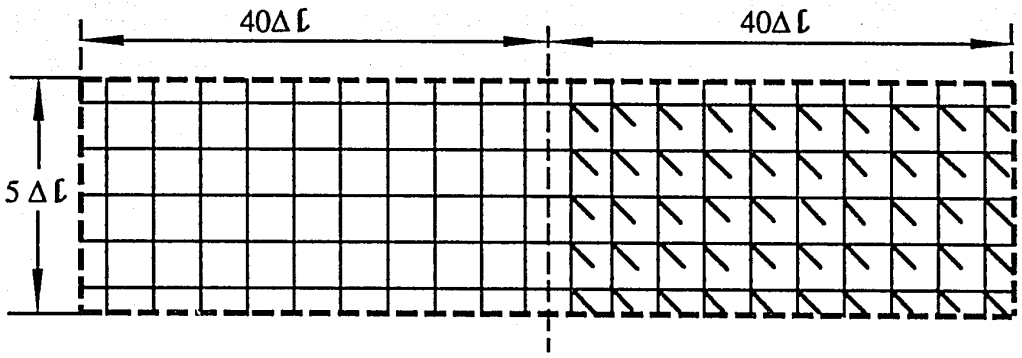

(b)

Fig. 2.4: (a) The top view of an inhomogeneous resonator which is enclosed by magnetic walls.

(b) The TLM mesh for the structure (a). The stubs can be either open-circuited or terminated with capacitances. $\Delta\ell$ =0.25 mm.

– – – – – – Magnetic Wall

ε_r	f_{01} (GHz)	C_1 (10^{-3}pF)	f_{02} (GHz)	f_a (GHz)	$\frac{\lvert f_a - f_{01} \rvert}{f_a}$ (%)	$\frac{\lvert f_a - f_{02} \rvert}{f_a}$ (%)
3	5.80	4.427	5.80	5.856	0.24	0.15
4	5.53	8.854	5.53	5.488	0.51	0.15
5	5.27	13.28	5.28	5.195	0.87	0.67
6	4.91	17.71	4.94	4.944	1.50	0.89
7	4.85	22.14	4.82	4.723	1.30	0.66
8	4.60	26.56	4.60	4.527	0.44	0.44
9	4.25	30.99	4.25	4.320	1.85	1.39
10	4.03	35.42	4.15	4.191	0.02	0.98
11	3.87	39.84	3.90	4.046	0.64	0.64
12	3.81	44.27	3.83	3.914	0.87	1.38
13	3.65	48.70	3.66	3.793	1.10	1.66
14	3.50	53.13	3.53	3.682	2.23	2.23

Table 2.2 : The simulation and analytical results for the first resonant frequency of the resonator in Fig 2.4. f_{01} is obtained when the stubs in Fig. 2.4 are open-circuited and f_{02} is obtained when the stubs are terminated with capacitances.

2.3.3 Simulation of a Lumped Capacitance in a Medium of an Arbitary Relative Permittivity

In section 2.3.1, a lumped capacitance in a medium which has a relative permittivity of 2 is simulated sucessfully with the new model. To make it general, a stub with loading capacitance should be able to simulate a lumped capacitance in a medium which has an arbitary relative permittivity. Since there is only one capacitance stub for each node, both the lumped capacitance and the capacitance for the relative permittivity must be added to the end of the stub. Based on the results from the previous two subsections, for the lumped capacitance C_n in a medium with a relative permittivity of $\epsilon_r \geq 2$, the loading capacitance at the end of stubs should be:

$$C_l = 2C_n + 2\epsilon_0(\epsilon_r - 2)\,\Delta\, l \quad . \tag{2.23}$$

2.4 Accuracy and Stability

2.4.1 Open-circuited Stub

Since the TLM mesh containing open-circuited stubs consists only of lossless transmission lines, it is unconditionally stable.

The error of the open-ended stub model is due to the distributed inductance in the stub transmission line. The admittance of the stub added to the node is given by steady-state transmission-line theory as:

$$\begin{aligned} Y_{ad} &= j\frac{2C_{ad}}{\Delta t} tan\frac{\omega\,\Delta\, t}{2} \\ &= j\frac{2C_{ad}}{\Delta t}[\frac{\omega\,\Delta\, t}{2} + \frac{1}{3}(\frac{\omega\,\Delta\, t}{2})^3 + ...] \\ &= j\omega C_{ad} + jZ_0\frac{\omega^3\,\Delta\, t^3}{24} + \ldots \quad , \end{aligned} \tag{2.24}$$

where

$$C_{ad} = C\,\Delta\, l$$

$$\Delta t = \sqrt{LC}\,\Delta l$$
$$Z_0 = \frac{\Delta t}{2C_{ad}} .$$

Here, Δl is the stub length, and C and L are the capacitance and inductance per unit length of the link lines, respectively.

Comparing (2.24) with the admittance Y_s that should be added to the nodes

$$Y_s = j\omega C_{ad} \quad , \tag{2.25}$$

The first-order error of the admittance is:

$$\Delta Y = Y_{ad} - Y_s = jZ_0\frac{\omega^3\,\Delta t^3}{24} = Z_0\frac{\pi^3}{3}(\frac{\Delta l}{\lambda})^3 \tag{2.26}$$

Thus, the error in modelling the capacitance by an open-circuited stub is of order Δt^3. The error is also proportional to ω^3. At relatively low frequencies ($\frac{\Delta l}{\lambda} \ll 1$), it is fairly small and negligible.

2.4.2 Stub Loaded with Capacitance and Resistance

When we discussed the properties of the capacitance-loaded stubs, we had already derived the difference equation for the reflection coefficient algorithm from the differential equation governing the capacitance as shown in section 2.1. The same approach can be used to model the case where a shunt conductance is placed in parallel with the capacitance to simulate losses (see figure 2.5).

The voltage and current in the system are governed by:

$$i - i_1 = C_l\frac{dv}{dt} \tag{2.27}$$
$$v = i_1 R_l \tag{2.28}$$

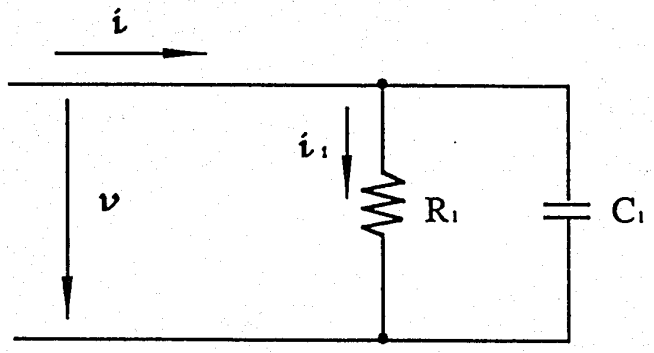

Fig. 2.5 : General lumped element terminating the stub

When discretizing and linearizing these expressions, we have the option to choose the forward or backward difference.

For the backward difference, we have:

$$ {}_{k+1}V - {}_{k}V = \frac{{}_{k}I}{C_l}\Delta t - \frac{{}_{k}V}{R_l C_l}\Delta t \tag{2.29} $$

Since

$$ \begin{aligned} {}_{k}V &= {}_{k}V_5^r + {}_{k}V_5^i \\ {}_{k}I &= Y_r[{}_{k}V_5^r - {}_{k}V_5^i] \quad , \end{aligned} \tag{2.30} $$

substituting (2.30) into (2.29) yields

$$ {}_{k+1}V_5^r - {}_{k}V_5^r - \frac{Y_r\Delta t}{C_l}\,{}_{k}V_5^r + \frac{\Delta t}{R_l C_l}\,{}_{k}V_5^r = {}_{k}V_5^i - {}_{k+1}V_5^i - \frac{Y_r\Delta t}{C_l}\,{}_{k}V_5^i - \frac{\Delta t}{R_l C_l}\,{}_{k}V_5^r \quad . \tag{2.31} $$

Since we have discretized the nonlinear differential equation into a difference equation, every stub in the TLM mesh can be treated as a small linear discrete-time system. As the system can be described by the linear constant-coefficient difference equation (2.31), the stability of the stub in the TLM mesh can be analyzed as follows. Considering ${}_{k}V^r$

and ${}_kV^i$ as the input and output sequence, respectively, and taking the Z-transform of the above equation gives:

$$(z - 1 - \frac{Y_r \Delta t}{C_l} + \frac{\Delta t}{R_l C_l})\ V_z^r = (1 - z - \frac{Y_r \Delta t}{C_l} - \frac{\Delta t}{R_l C_l})\ V_z^i \tag{2.32}$$

where

$$V_z^r = \mathcal{Z}[{}_kV^r] \tag{2.33}$$

$$V_z^i = \mathcal{Z}[{}_kV^i] \tag{2.34}$$

Hence, the equivalent system function $H(z)$ will be

$$H(z) = \frac{V_z^i}{V_z^r} = \frac{z - 1 - \frac{Y_r \Delta t}{C_l} + \frac{\Delta t}{R_l C_l}}{1 - z - \frac{Y_r \Delta t}{C_l} - \frac{\Delta t}{R_l C_l}} \tag{2.35}$$

For a causal system, the Region of Convergence (ROC) will be outside the outmost pole. Also, if the system is stable, the impulse response $h[n]$ must be absolutely summable [17], i.e.,

$$\sum_{n=-\infty}^{\infty} |h[n]| < \infty \quad . \tag{2.36}$$

It is equivalent to

$$\sum_{n=-\infty}^{\infty} |h[n] z^{-n}| < \infty \quad , \qquad |z| = 1 \quad . \tag{2.37}$$

So the condition of stability is equivalent to the condition that the ROC of $H(z)$ includes the unit circle. For a causal and stable system, the ROC of the $H(z)$ should include the unit circle and all area outside the unit circle on the Z-plane, i.e. all the poles of $H(z)$ should be inside the unit circle.

For this case, we have only one pole:

$$z = 1 - \frac{Y_r \Delta t}{C_l} - \frac{\Delta t}{R_l C_l} \quad . \tag{2.38}$$

To satisfy the stable condition

$$|z| < 1 \tag{2.39}$$

we must have

$$0.0 < \frac{Y_r \Delta t}{C_l} + \frac{\Delta t}{R_l C_l} < 2.0 \tag{2.40}$$

Using the backward difference, the simulation might get unstable if the above condition is not satisfied.

For the forward difference, following the same procedure as above, we get the stable condition as:

$$Y_r \frac{\Delta t}{C_l} + \frac{\Delta t}{R_l C_l} > 0.0 \tag{2.41}$$

This will be automatically satisfied if all parameters in this equation are positive real. This is the reason why we choose the forward difference in capacitance simulation whenever possible.

2.4.3 The Low-pass Effect of the Integration

Figures 2.6 to 2.8 show several frequency responses for the structure in figure 2.4(a) from the TLM simulation done with different stub models, different mesh sizes, or different value of ϵ_r.

Comparing figure 2.6 (a) with figure 2.6 (b), they have the peaks at the same frequencies, but the high-frequency components in (a) are suppressed in amplitude. This is not very serious for eigenvalue problems as long as the peaks are still distinguishable. But for the simulation of time-dependent components such as varactor diodes which will be discussed in the next chapter, it is a fatal problem. This low-pass effect of the stub loaded with capacitance is due to the integration of the differential equation, since the integration averages the rapidly varying components.

Comparing figure 2.7(a) with (b), it appears that the suppression of high frequency components gets stronger when the loading capacitance C_l is increased.

Comparing figure 2.8(a) with (b), a difference in amplitude is observable from 5 GHz onward; when a finer mesh is used, results are almost identical for frequencies below 10 GHz. So, a wider useful frequency range can be obtained for the stub loaded with capacitance by using a finer TLM mesh. In order to get the right solution for both frequency and amplitude at relatively low frequencies ($\frac{\Delta l}{\lambda} \ll 1$), the open-circuited stub model gives a

useful frequency range, and the stub loaded with capacitance requires more computational effort.

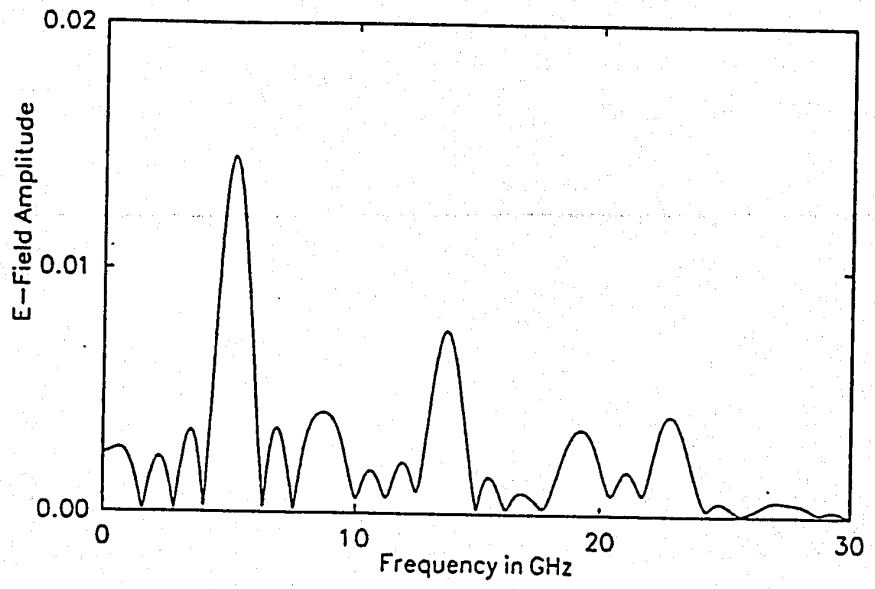

(a)

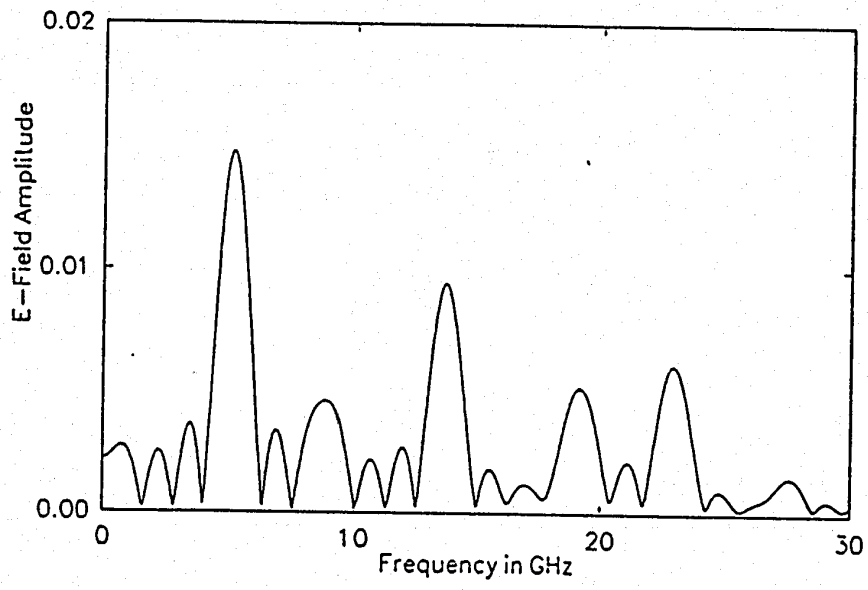

(b)

Fig. 2.6 (a) Frequency response for the structure in fig.2.4 (a). Simulation is done by capacitance-loaded stub model. $\varepsilon_r = 5$, $\Delta l = 0.25$ mm.
(b) Frequency response for the structure in fig.2.4 (a). Simulation is done by open-circuited stub model. $\varepsilon_r = 5$, $\Delta l = 0.25$ mm.

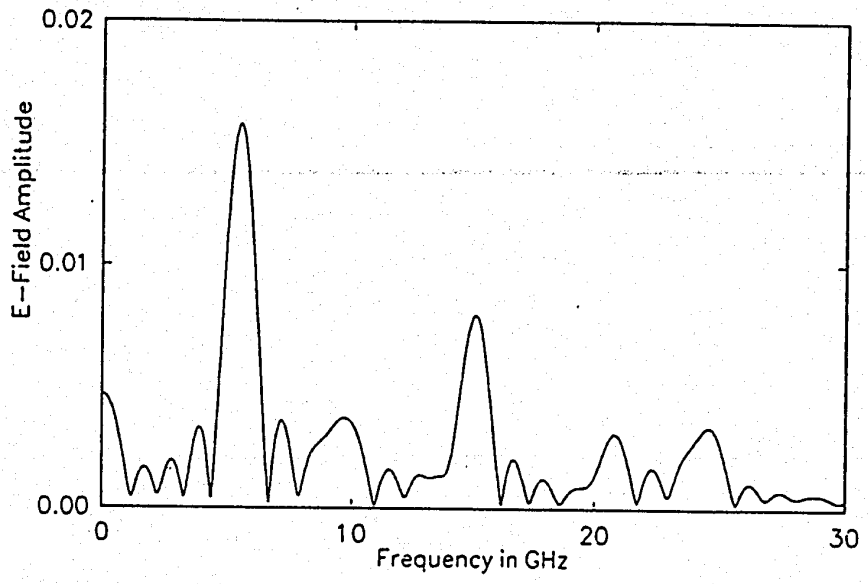

(a)

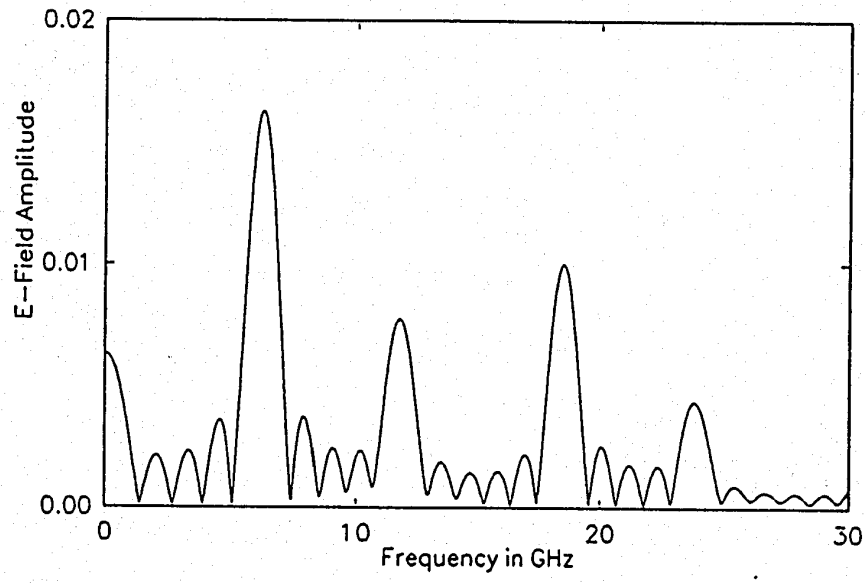

(b)

Fig. 2.7 (a) Frequency response for the structure in fig.2.4 (a). Simulation is done by capacitance-loaded stub model. ε_r =2.2, Δl = 0.25 mm.
(b) Frequency response for the structure in fig.2.4 (a). Simulation is done by capacitance-loaded stub model. ε_r = 4, Δl = 0.25 mm

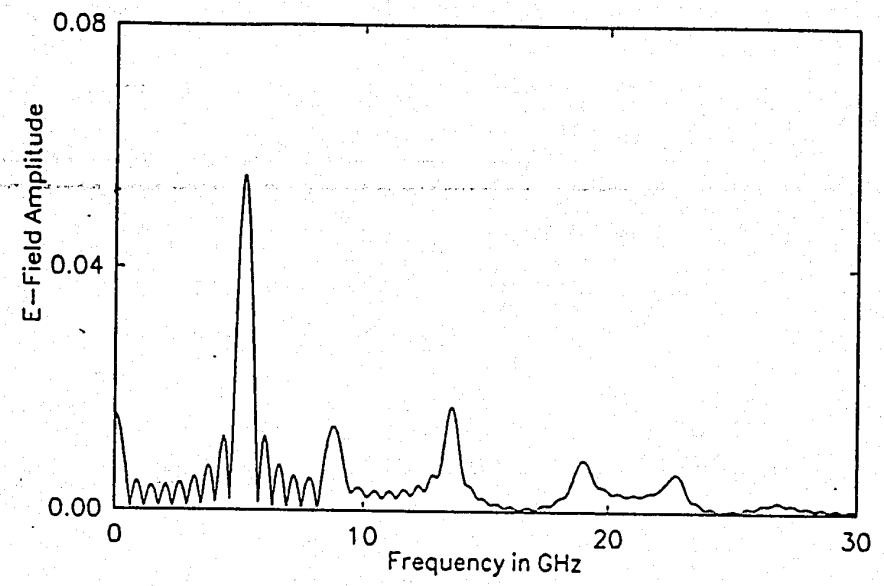

(a)

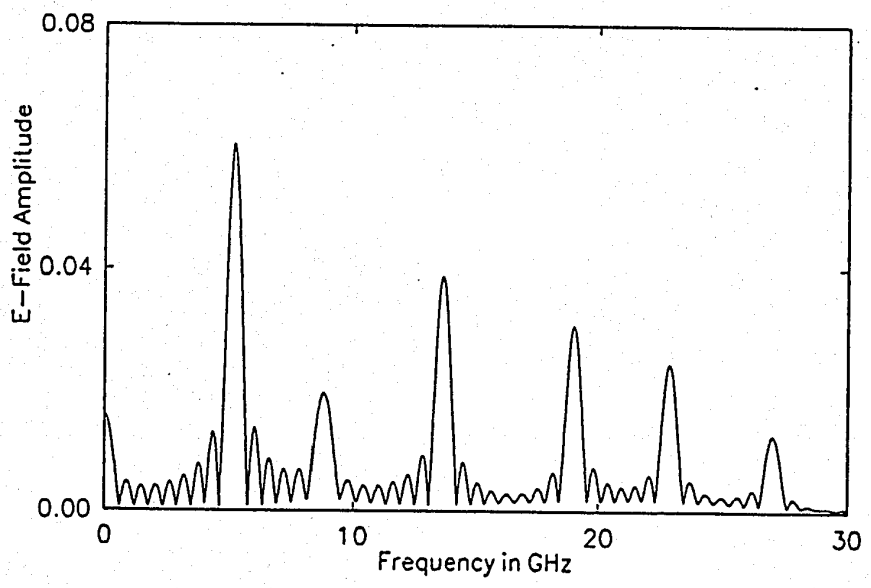

(b)

Fig. 2.8 (a) Frequency response for the structure in fig.2.4 (a). Simulation is done by capacitance-loaded stub model. $\varepsilon_r = 5$, $\Delta l = 0.5$ mm.
(b) Frequency response for the structure in fig.2.4 (a). Simulation is done by open-circuited stub model. $\varepsilon_r = 5$, $\Delta l = 0.5$ mm.

2.5 Conclusion

In this chapter, the stub loaded with constant capacitance is described and used for the simulation of lumped capacitance and relative permittivity. The results agree with the results obtained with the open-circuited stub model and the analytical results for relatively low frequencies ($\frac{\Delta l}{\lambda} \ll 1$), while at high frequencies the two models give different results due to their different dispersion characteristics. This new model provides us with a new way to simulate voltage-dependent capacitance.

Chapter 3

Simulation of Voltage-Dependent Capacitance

3.1 Introduction

In this chapter, a review of the simulation of varactor diodes is given. Several modifications are suggested for the simulation of a varactor diode by an open-circuited stub model. A new model for the varactor diode is developed, based on the model of a stub terminated with a nonlinear lumped circuit. Both models are used for the simulation of a simple nonlinear element in a TLM mesh, and the results agree well. The simulation of a varactor diode by a capacitance-loaded stub model is also discussed. Simulations of a varactor diode done with differents stub models give similar results.

3.2 Review

In 2D-TLM simulation, nonlinear structures and devices have been modelled in two different ways. The first model is discussed both in reference [14] and [20]. A voltage-dependent capacitance (varactor) embedded in a microstrip circuit has been modelled in the time domain by a submesh which represents a medium with variable permittivity and conductivity (proposed by Dr. Harrison). The permittivity and conductivity depend upon the equivalent circuit of the varactor diode, so that the submesh in the TLM mesh will behave in the same way as the varactor diode in the microwave circuit.

The implementation of this method includes two steps[14]:

1. Transform the varactor diode into a submesh which has voltage-dependent permittivity and conductivity.

2. Update the voltage-dependent admittance of the open-circuited stub y_0 and the voltage-dependent conductivity of the loss stub g_0 in the TLM submesh.

These steps will be detailed below.

1. **Transform the varactor diode into a submesh which has voltage-dependent permittivity and conductivity.**

   The equivalent circuit for the varactor diode is shown in figure 3.1. For a Schottky barriers varactor diode, the main parameters such as the depletion-layer capacitance $C_d(v)$, the diffusion capacitance $C_{di}(v)$ and the voltage-dependent resistance $R(v)$ are given in [20] as

$$\begin{aligned} C_d(v) &= \frac{C_{j0}}{\sqrt{1-\frac{v}{\phi_0}}} \qquad \text{for} \quad v < \phi_0/2 \\ &= \sqrt{2}C_{j0}(\frac{v}{\phi_0}+\frac{1}{2}) \qquad \text{for} \quad v \geq \phi_0/2 \end{aligned} \tag{3.1}$$

$$C_{di}(v) = C_{d0}exp(\frac{\epsilon v}{kT}) \tag{3.2}$$

$$R(v) = (\frac{kT}{\epsilon I_s})\exp(-\frac{\epsilon v}{kT}) \tag{3.3}$$

   where C_{j0} is the zero-bias capacitance, ϕ_0 is the built-in potential, I_s is the saturation current and v is the junction voltage. The linear approximation of $C_d(v)$ is used when $v \geq \phi_0/2$ in oder to avoid the singularity which might crush the numerical simulation.

   e= Electron charge

   k=Boltzmann's constant

   T= Temperature in K

   So, the total voltage-dependent capacitance $C(v)$ is:

$$C(v) = C_d + C_{di} + C_p \tag{3.4}$$

The package capacitance C_p can also be included if necessary.

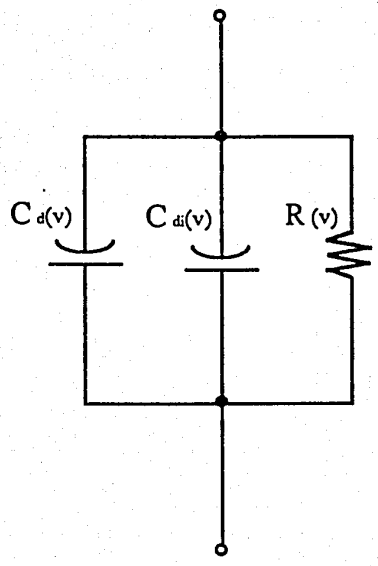

Fig. 3.1: The equivalent circuit for the varactor diode

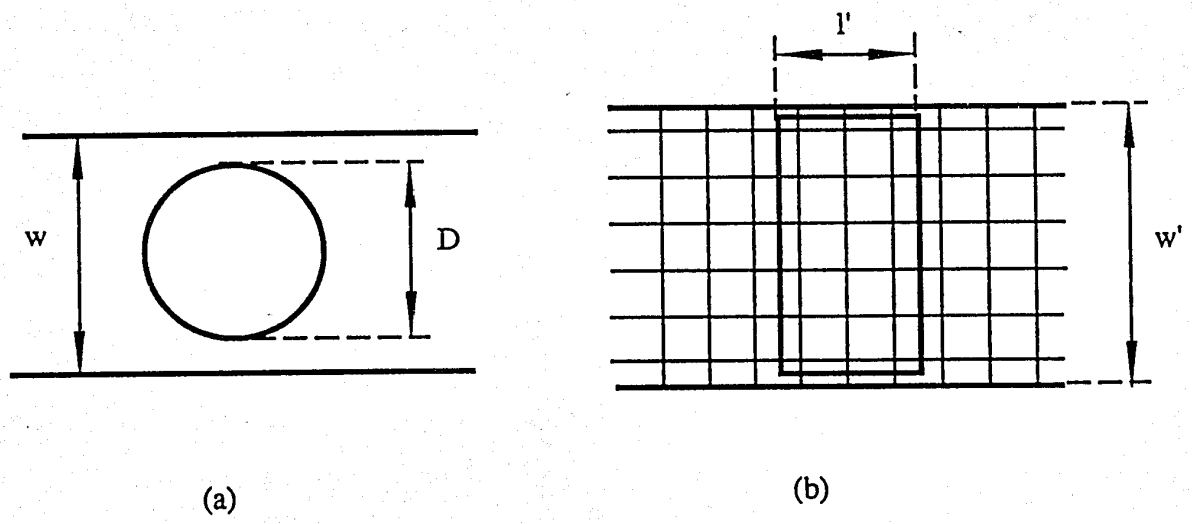

Fig. 3.2: (a) The varactor diode embedded in microstrip
(b) TLM mesh with the submesh simulating the varactor diode: all nodes inside the rectangular box are equipped with reactive and loss stubs to model the diode characteristics.

In two dimensions, the microstrip can be modelled for relatively low frequencies ($\frac{\Delta l}{\lambda} \ll 1$) by a parallel-plate transmission line which is easily represented by a standard 2D-TLM mesh. The voltage-dependent capacitance of the varactor diode can be modelled as a small subregion with voltage-dependent permittivity and conductivity embedded in the 2D-TLM mesh.

As shown in figure 3.2, it is essential that the area of the small submesh is equal to the area of the diode package. w' is different from the width of microstrip w for the compensation of fringing effect. l' will be decided by:

$$l' = \frac{\pi D^2}{4w'} \tag{3.5}$$

Using the concept of the parallel-plate transmission line, the capacitance and resistance of the submesh can be calculated by equations (3.6) and (3.7), respectively.

$$C_s = \frac{\epsilon_0 \epsilon_r A}{h} \tag{3.6}$$

$$R_s = \frac{h}{A\sigma} \tag{3.7}$$

where

A =the area of the submesh

h =the substrate thickness

ϵ_r= the relative permittivity of the submesh

σ= the conductivity of the submesh.

To make the capacitance and resistance of the submesh equal to those of the varactor diode, the following relationship can be established by comparing equation(3.4) with (3.6) and (3.3) with (3.7):

$$\epsilon_r(v) = \frac{C(v)h}{A\epsilon_0} \tag{3.8}$$

$$\sigma(v) = \frac{h}{AR(v)} \tag{3.9}$$

In the TLM simulation, the relative permittivity of the mesh can only be greater than 1, so the capacitance that can be simulated by the submesh will be:

$$C(v) \geq \frac{A}{h}\epsilon_0 \tag{3.10}$$

For the case of $h = \Delta l$, one node will only be able to simulate a capacitance greater than $\epsilon_0 \Delta l$.

2. **Update the voltage-dependent admittance of the open-circuited stub y_0 and the voltage-dependent conductivity of the loss stub g_0 in the TLM mesh**

   In the first step, the varactor diode is transformed into a TLM submesh; meanwhile, the change of capacitance and resistance is equivalent to the change of the permittivity and conductivity of the submesh. This can be implemented in a TLM simulation by updating the voltage-dependent characteristic admittance of the open-circuited stub y_0 and the voltage-dependent conductivity of the loss stub g_0 in each interation according to the permittivity and conductivity of the submesh determined in the previous iteration:

$$y_0(v) = 4[\epsilon_r(v) - 1] \tag{3.11}$$

$$g_0(v) = \sqrt{2}\sigma(v)\ \Delta l\ \eta_0 \quad . \tag{3.12}$$

The method has been used in the simulation of a varactor diode frequency multiplier and a divider in reference [14].

The second method, which is discussed in reference [19], models active and nonlinear microwave structures by a subregion in the TLM mesh. In the subregion, the shunt nodes are equipped with additional stubs which are terminated with lumped circuit elements. The impulses reflected from the stubs can be obtained from a recursive formula which

amounts to numerically integrating the nonlinear differential equation that governs the lumped circuit elements. The important advantage of this method is that the model can suppress the high-frequency spurious solutions in the TLM mesh by properly representing the intrinsic cutoff frequency of the lumped circuit. In section 3.3, this idea will be used to develop the algorithm for the simulation of varactor diodes.

3.3 Several Modifications for the Simulation of a Microstrip Multiplier with the Open-Circuited Stub Model

The following aspects will be discussed in detail below:

1. The effect of the package
2. Energy conservation in the open-circuited stub model.

1. **The effect of the package**

   When we replace the lumped varactor by a submesh which contains several independent nodes, these nodes will have different voltages during the iteration. In real situations, the chips are always well packaged. Therefore, there is only one voltage applied to the whole varactor. In order to be close to the practical condition of the varactor, instead of using the voltage on each node to get the local permittivity and conductivity, the average of the voltages on the nodes can be computed and assumed to be uniform within the submesh. With this voltage, a unique relative permittivity and conductivity for all the nodes in the submesh can be obtained from equations (3.8) and (3.9).

2. **Energy conservation in the open-circuited stub**

   As shown in figure 3.3, when the impulse ${}_kV_5^r$ enters the open-circuited stub, the stub has the characteristic admittance ${}_ky_0$. Since the stubs are open-circuited, the impulse will be reflected back to the node in the same amplitude. But at this time, the characteristic admittance of the stub has already been changed to ${}_{k+1}y_0$. Considering the energy fed in stub (P_i) and the energy reflected back from stub (P_r), we have:

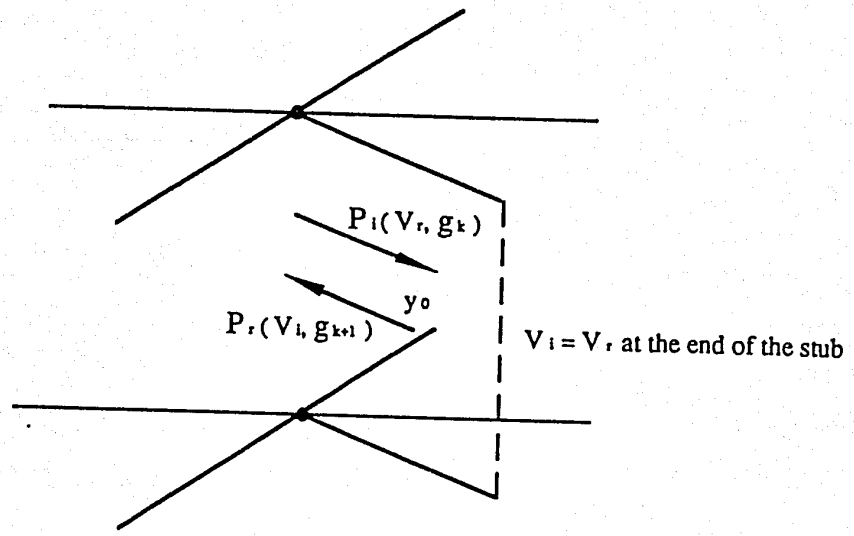

Fig. 3.3: Shunt node with open-terminated stub

$$P_i \propto {}_k y_0 \, {}_k V_5^{r2} \tag{3.13}$$

$$P_r \propto {}_{k+1} y_0 \, {}_k V_5^{r2} \tag{3.14}$$

In nonlinear cases, ${}_k y_0$ does not equal ${}_{k+1} y_0$ and thus P_r will not be the same as P_i. Since the stub itself is only a short lossless transmission line, the difference between P_i and P_r violates the law of energy conservation. In order to keep energy conserved on the stubs, we have to keep $P_i = P_r$ in each iteration. This can be done by modifying the P_r corresponding to the change of the characteristic admittance of the stub or the change of the permittivity in the submesh.

Substituting the expression of y_0 (refer to equation(3.11)) into the above equations (3.13) and (3.14) , we have:

$$P_i \propto ({}_k\epsilon_r - 1) \, {}_k V_5^{r2}$$

$$P_r \propto ({}_{k+1}\epsilon_r - 1) \, {}_{k+1} V_5^{i2}$$

If $P_i = P_r$, then

$$({}_k\epsilon_r - 1)\ {}_kV_5^{r2} = ({}_{k+1}\epsilon_r - 1)\ {}_{k+1}V_5^{i2} \tag{3.15}$$

${}_{k+1}V_5^i$ will be:

$${}_{k+1}V_5^i = \sqrt{\frac{{}_k\epsilon_r - 1}{{}_{k+1}\epsilon_r - 1}}\ {}_kV_5^r \tag{3.16}$$

The necessity of this modification will be further proved by the simulation results in section 3.5.

3.4 Simulation of an Voltage-dependent Capacitance with a Stub Loaded with Variable Capacitance

As shown in the last chapter, lumped capacitances have been simulated by a stub loaded with capacitance. This stub model also can be used to simulate nonlinear reactive components. The details of this procedure are shown below.

1. **Determine the lumped element which terminates the stub**

   The intrinsic impedance of the conventional TLM mesh is always $\frac{1}{\sqrt{2}}$ times smaller than the impedance it simulates, and the frequency is compensated by the same factor after discrete Fourier transformation. In order to add a lumped voltage-dependent capacitance $C(v)$, the capacitance loaded at the end of the stub should be:

   $$C_{l(v)} = 2C(v) \tag{3.17}$$

   To represent the capacitance, we must also realize that the TLM shunt node and the stub itself have already a certain capacitance of their own. For one TLM shunt node with a stub ($y_0 = 4$), this capacitance is $4\epsilon_0 \triangle l$, and it must be deducted from the capacitance at the end of stub. Finally, we have:

   $$C_{l(v)} = 2C(v) - 4\epsilon_0 \triangle l \tag{3.18}$$

With the capacitance-loaded stub model, one node can only represent a capacitance greater than $4\epsilon_0 \Delta l$. This lower limitation is four times greater than that with an open-circuited stub model. Fortunately, both limitations are fairly small for the simulation of a real varactor diode.

2. **Set up the recursive formula for the impulse reflected at the end of the stub**

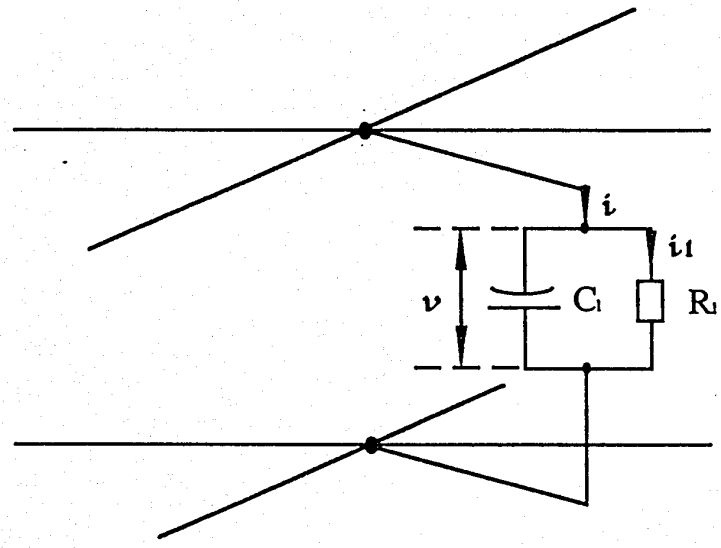

Fig. 3.4.: Shunt TLM node with stub terminated by variable capacitance and resistance

Referring to figure 3.4, we have:

$$i - i_1 = \frac{d[C_l(v)v]}{dt} \tag{3.19}$$

$$i_1 = \frac{v}{R_l(v)} \tag{3.20}$$

Combining equations (3.19) and (3.20),

$$i - \frac{v}{R_l(v)} = C_l(v)\frac{dv}{dt} + v\frac{dC_l(v)}{dv}\frac{dv}{dt} \tag{3.21}$$

$$\frac{dv}{dt} = \frac{i - \frac{v}{R_l(v)}}{C_l(v) + v\frac{dC_l(v)}{dv}} \tag{3.22}$$

Replacing $\frac{dv}{dt}$ in equation (3.22) by a finite difference, we get

$$ {}_{k+1}V - {}_{k}V = \frac{{}_{k}I - \frac{{}_{k}V}{{}_{k}R_l}}{{}_{k}C_l + {}_{k}V\alpha_k} \Delta t \tag{3.23} $$

$$ \alpha_k = \frac{dC_l}{dv}|_{v={}_{k}V} \quad . \tag{3.24} $$

Since we have equations (2.4) and (2.5)

$$ \begin{aligned} {}_{k}V &= {}_{k}V^r + {}_{k}V^i \\ {}_{k}I &= Y_r({}_{k}V^r - {}_{k}V^i) \quad . \end{aligned} $$

Substituting them into (3.23), the recursive formula is obtained:

$$ {}_{k+1}V^i = {}_{k}V + \frac{{}_{k}I - \frac{{}_{k}V}{{}_{k}R_l}}{Ct} {}_{k}V - {}_{k+1}V^r \quad . \tag{3.25} $$

For lossless cases:

$$ {}_{k+1}V^i = (1 + \frac{{}_{k}I}{Ct}){}_{k}V - {}_{k+1}V^r \tag{3.26} $$

where

$$ Ct = \frac{{}_{k}C_l + ({}_{k}V^r + {}_{k}V^i)\alpha_k}{\Delta t} \quad . \tag{3.27} $$

3.5 Comparing the Different Models in the Simulation of a Voltage-Dependent Capacitance

A simple TLM mesh is shown in figure 3.5. At node B, a voltage-dependent capacitance is inserted. With a sinusoidal excitation at node A, the simulation results are extracted from the field amplitude at the output point C.

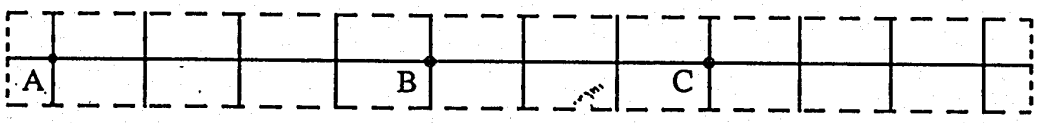

Figure 3.5: A TLM mesh with a voltage-dependent capacitance inserted at B.

— — — — — — Magnetic wall

---------- Absorbing boundary

The voltage-dependent capacitance of a Schottky barriers varactor diode is given by the expression [8]:

$$\begin{aligned} C(v) &= \frac{C_{j0}}{\sqrt{1-\frac{v}{\phi_0}}} \qquad \text{for} \quad v < \phi_0/2 \\ &= \sqrt{2}C_{j0}(\frac{v}{\phi_0}+\frac{1}{2}) \qquad \text{for} \quad v \geq \phi_0/2 \quad . \end{aligned}$$

The parameters for the varactor diode are chosen as below. Since we want to compare the behaviours of the two different stubs in simulation of voltage-dependent capacitance, here I_s is assumed to be zero.

$$C_{j0} = 5.5\,(pF)$$
$$\phi_0 = 0.7\,(V)$$

With the normalized input frequency at $\frac{\Delta l}{\lambda} = 0.0005$, the frequency domain responses of this structure has been obtained with different models. Comparing the results in figures 3.6(a) to (d), we find:

1. With the capacitance-loaded stub model, the results obtained are very close to the

results obtained from the simulation done by the open-circuited stub model after modification for energy conservation.

2. The results obtained from the simulation done by open-circuited stub model without the modification are very close to the results obtained from the simulation done by the capacitance-loaded stub model with $\frac{dC_l}{dv}$ equal to zero.

Since $\frac{dC_l}{dv}$ is not zero in nonlinear cases, setting $\frac{dC_l}{dv}$ to zero will make the capacitance-loaded stub model less accurate. Based on this, with the above two clues, we can say that the modification for energy conservation makes the open-circuited stub model more accurate.

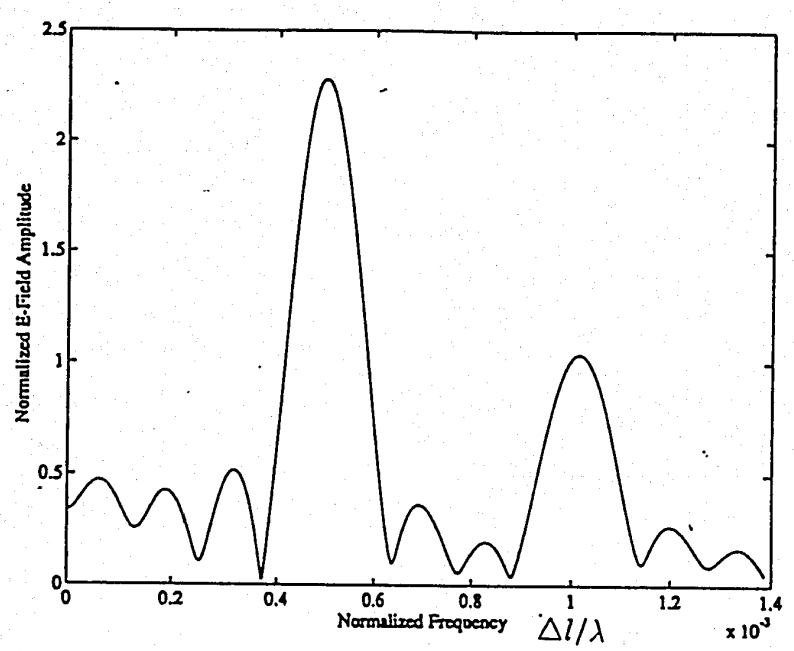

Fig.3.6 (a): The frequency response obtained with the modified open-circuited stub model

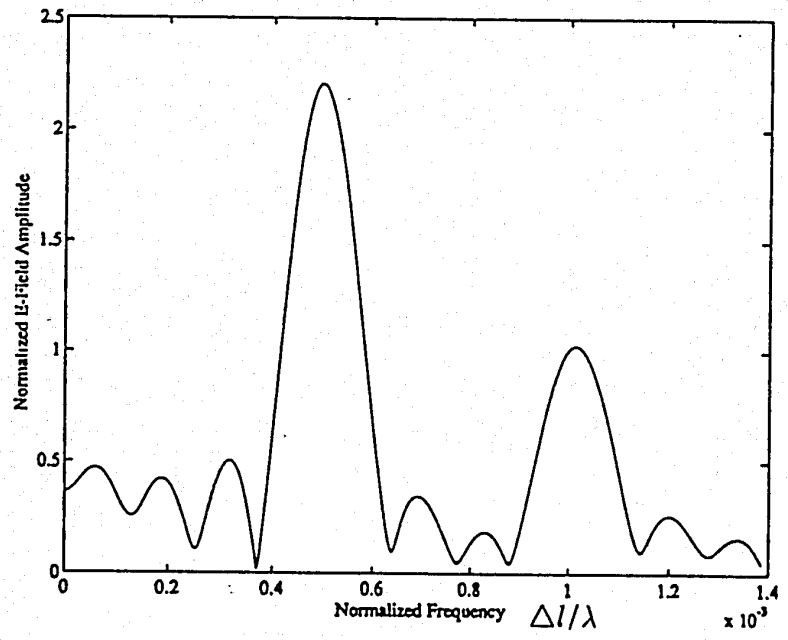

Fig.3.6 (b): The frequency response obtained with the capacitance-loaded stub model

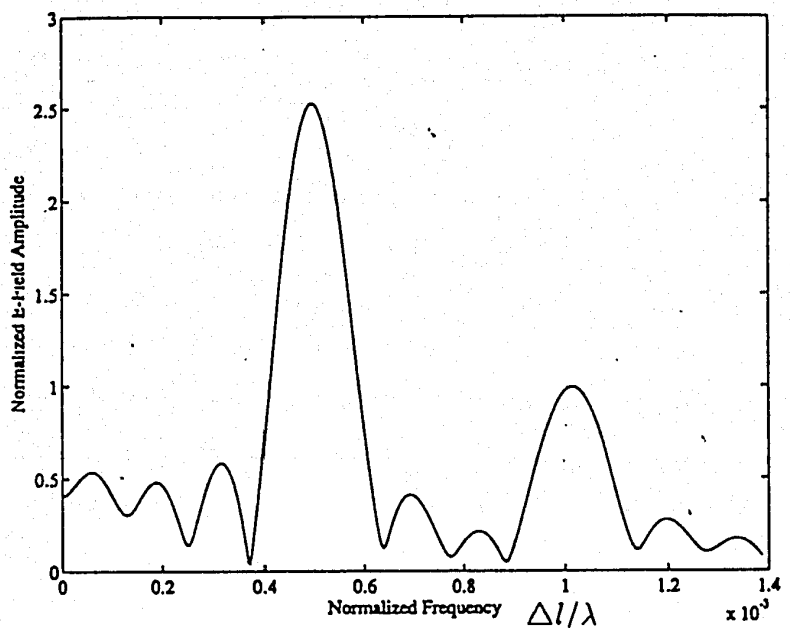

Fig.3.6 (c): The frequency response obtained with the open-circuited stub model without modification for energy conservation.

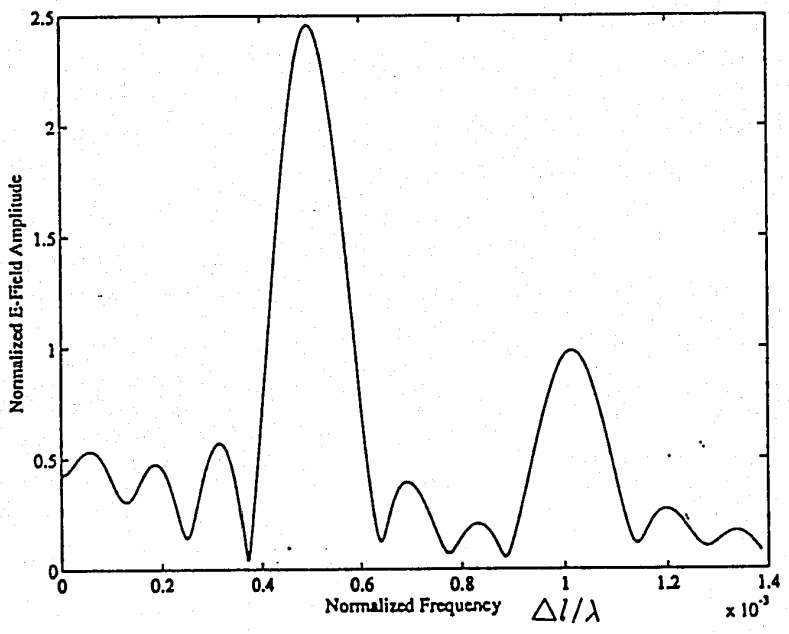

Fig.3.6 (d): The frequency response obtained with the capacitance-loaded stub model, while C_t is set to zero during the iterations.

3.6 Simulation of a Microstrip Circuit with a Varactor Diode with the Capacitance-loaded Stub Model

Based on the fact that both stub models work well for the simulation of voltage-dependent capacitances, both models should work well for the simulation of a real varactor diode. The simulation of a real varactor diode in a microstrip circuit has been performed using the open-circuited stub model [14]. It can be done by the capacitance-loaded stub model too. In this section, the simulation of a real varactor diode in a microstrip circuit by stubs terminated with lumpeded circuit will be discussed in detail. Simulation results for a simple mutiplier obtained with different models will be compared.

Transformation of a microstrip circuit into a TLM mesh with a submesh for the varactor diode has already been described in section 3.2. Then we only need to determine the capacitance C_l and resistance R_l at the end of stubs.

Assuming that the voltage is applied in the y direction and that the TLM mesh is in the x-z plane, then all the capacitors added to the nodes in the submesh are connected in parallel. Distributing the capacitance $C(v)$ and resistance $R(v)$ of the varactor diode over the submesh in the 2D-TLM mesh and including the effect of the height of the substrate h, each node in the submesh will get an additional capacitance C_n and resistance R_n.

$$C_n = \frac{C(v)}{N}\frac{h}{\Delta l} \tag{3.28}$$

$$R_n = R(v)N\frac{\Delta l}{h} \quad . \tag{3.29}$$

Considering the lower intrinsic impedance of the 2D-TLM mesh and the capacitance of the TLM mesh itself, the capacitance and resistance loaded on the end of the stubs in the submesh should be:

$$C_l = 2C_n - 4\epsilon_0\Delta l \tag{3.30}$$

$$R_l = \frac{R_n}{\sqrt{2}} \quad . \tag{3.31}$$

Substituting equation (3.28) and (3.29) into (3.30) and (3.31), respectively, we have

$$C_l = 2\frac{C(v)}{N}\frac{h}{\Delta l} - 4\epsilon_0\Delta l \tag{3.32}$$

$$R_l = \frac{R(v)N\,\Delta\,l}{h\sqrt{2}} \quad . \tag{3.33}$$

With the above equations and the formula in section 3.4, we are able to simulate the varactor diode in a microstrip circuit by the capacitance-loaded stub model.

For a simple mutiplier with a TLM mesh shown in figure 3.7, simulations are done by both the open-circuited and the capacitance-loaded stub model. The results in figure 3.8 are similar.

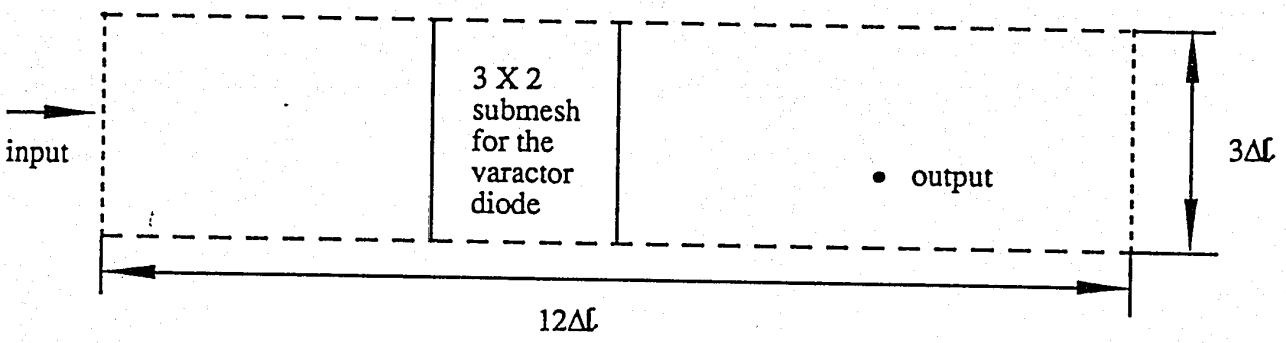

Figure 3.7: A TLM mesh with a submesh for a varactor diode.

— — — — — Magnetic wall

---------- Absorbing boundary

The substrate of the microstrip has a height of 0.3 mm and a relative permittivity of 10. Δl of the TLM mesh is 0.1 mm.

The parameters for a Schottky barriers varactor diode are:

$C_{j0} = 5.5\ (pF)$

$\phi_0 = 0.7\ (V)$

$I_s = 1.0 \times 10^{-18}\ (A)$

To involved the $R(v)$ in the simulation of varactor diode, here I_s is chosen not to be zero.

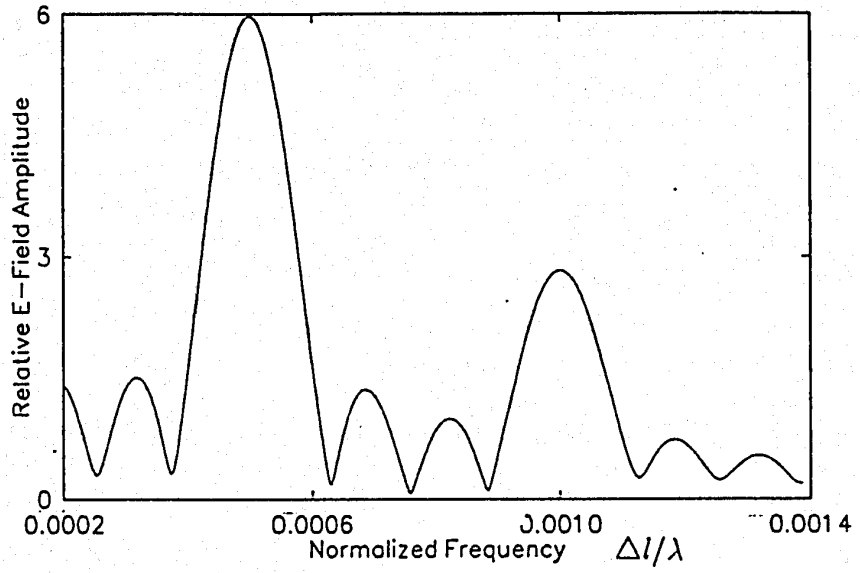

Fig.3.8 (a): The frequency response obtained with the open-circuited stub model

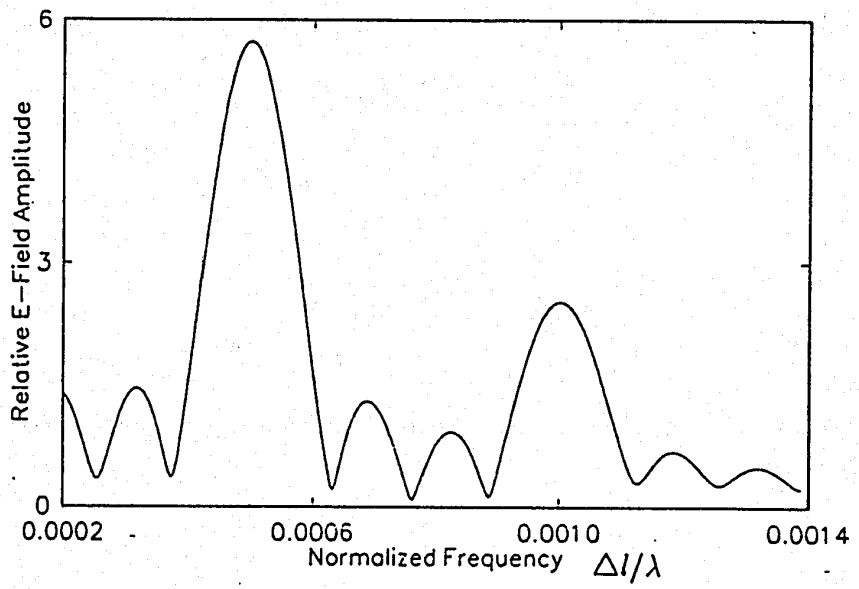

Fig.3.8 (b): The frequency response obtained with the capacitance-loaded stub model

3.7 The Equivalence of the Two Models in the Simulation of a Voltage-dependent Capacitance of a Varactor Diode

With the modifications to the open-circuited stub model, the relative permittivity of the submesh will be determined by equation(3.8):

$$\begin{aligned} \epsilon_r(v) &= \frac{C(v)h}{A\epsilon_0} \\ &= \frac{C(v)h}{N\Delta l^2\epsilon_0} \quad . \end{aligned} \tag{3.34}$$

Simulation of ϵ_r by a capacitance-loaded stub model has been discussed in section 2.3. Referring to equation (2.22), the capacitance loaded at the end of stub C_l and the ϵ_r are related by:

$$C_l = 2(\epsilon_r - 2)\epsilon_0 \Delta l \quad . \tag{3.35}$$

Substituting equation (3.34) into equation (3.35) we obtain

$$\begin{aligned} C_l &= 2(\epsilon_r(v) - 2)\epsilon_0 \Delta l \\ &= 2(\frac{C(v)h}{A\epsilon_0} - 2)\epsilon_0 \Delta l \\ &= 2\frac{C(v)h}{N\Delta l} - 4\epsilon_0 \Delta l \quad . \end{aligned} \tag{3.36}$$

The above equation derived from the formula used for the open-circuited stub model is exactly the same as the equation (3.32) which is used for capacitance-loaded stub model. This identity shows that simulations of the variable capacitance of varactor diode with the two different models are equivalent.

3.8 Conclusion

In this chapter, the voltage-dependent capacitance is sucessfully simulated by both the open-circuited and capacitance-loaded stub models. Based on it, two models are also

used to simulate the varactor diode embedded in a microstrip circuit. Comparing the two models, they both work well at relatively low frequencies ($\frac{\Delta l}{\lambda} \ll 1$). Both models have a lower limitation for the capacitance to be simulated. The limitation on the open-circuited stub model is smaller than the other. The capacitance-loaded stub model is more demanding in the case of fine TLM meshes. Since the very fine mesh is only needed for the submesh, a variable mesh size TLM mesh could be used for higher efficiencies in simulation. This technique is described in reference [2].

Chapter 4

Simulation of Series-Connected Capacitance

4.1 Introduction

In the previous chapters, open-circuited stubs have been used to simulate the lumped capacitance and varactor diode which are connected in parallel to the transmission line. The serial connection of the varactor diode has become popular because planar varactor diodes can be fabricated with anode and cathode contacts as integral parts of the transmission line. So, the insertion of the varactor diodes does not require any modification of the embedding circuit. Also, the serial connection makes it practical to increase the power handling capability by replacing the single diode with a number of diodes connected in series. In reference [7], a GaAs monolithic frequency doubler in which the varactor diode is connected in series with the transmission line is introduced. In this chapter, we provide another way to add the stubs into the TLM shunt node mesh. By using this technique, a capacitance or a varactor diode which is connected in series with the transmission lines can be simulated.

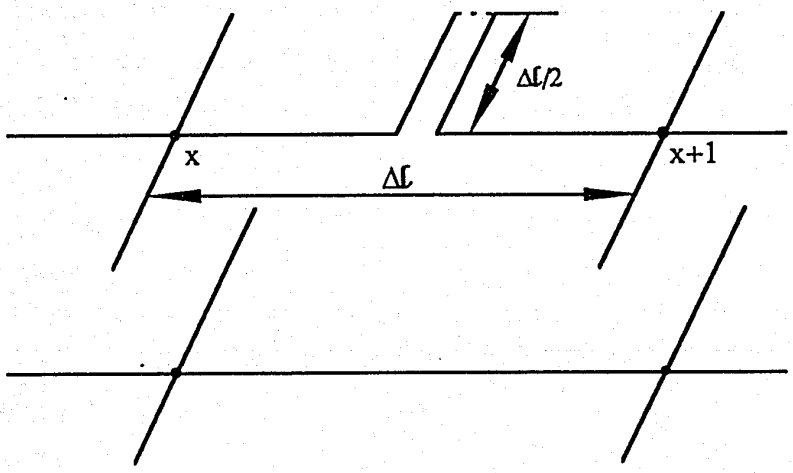

(a)

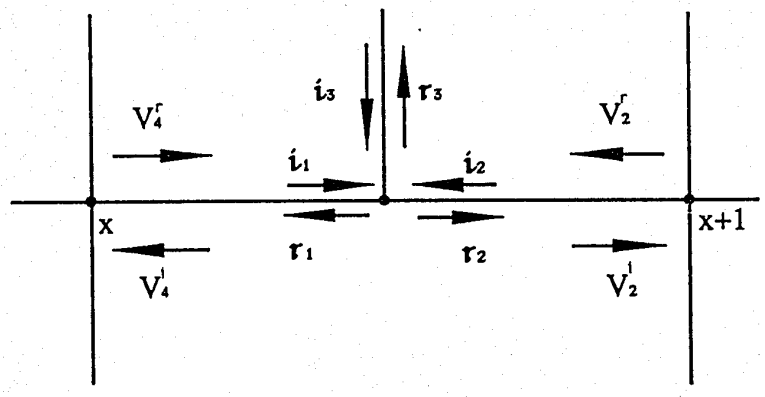

(b)

Fig. 4.1: (a) Open-circuited stub connected in series between two shunt nodes
(b) The transmission of the impulses on the structure given in (a)

4.2 The Scattering and Transmission in the TLM Mesh with Stubs between the Shunt Nodes

As described in the previous chapters, the lumped capacitance, which is connected in parallel to the transmission line, can be simulated by adding open-circuited stubs to the nodes in the shunt TLM mesh. Here, instead of adding the stubs to the nodes, we insert the open-circuited stubs half-way between the nodes. This structure, as shown in Figure 4.1, will be able to simulate capacitance which is connected in series with the transmission line.

The shunt nodes will work in the same way as before. But the voltage impulses will experience an additional scattering and transmission at the interface where the stubs are inserted. As shown in Figure 4.1, the stubs are inserted between the shunt nodes at x and $x+1$. At $\frac{\Delta t}{2}$ ($\Delta t = \frac{\Delta l}{c}$) after the scattering has happened at the shunt nodes, the voltage impulses will reach the stub: they are:

$$
\begin{aligned}
{}_k i_1 &= {}_k V_4^r(x) && (4.1)\\
{}_k i_2 &= {}_k V_2^r(x+1) && (4.2)\\
{}_k i_3 &= {}_{k-1} r_3 \ . && (4.3)
\end{aligned}
$$

Then they scatter at the stub, and produce ${}_k r_1$, ${}_k r_2$ and ${}_k r_3$. The S matrix will be derived in the next section.

$$
{}_k \begin{bmatrix} r_1 \\ r_2 \\ r_3 \end{bmatrix} = \begin{bmatrix} S \end{bmatrix} \cdot {}_k \begin{bmatrix} i_1 \\ i_2 \\ i_3 \end{bmatrix} \ .
$$

After another $\frac{\Delta t}{2}$ time interval, the ${}_k r_1$ and ${}_k r_2$ will reach the nodes at x and $x+1$, respectively, where we have:

$$
\begin{aligned}
{}_{k+1} V_4^i(x) &= {}_k r_1 && (4.4)\\
{}_{k+1} V_2^i(x+1) &= {}_k r_2 \ . && (4.5)
\end{aligned}
$$

Then the voltage impulses are scattered on the shunt nodes, and the above process will start again. Since no time is taken for the scattering at the stub, it takes an interval Δt for the period. We know that the time interval for the impulses travelling from one node to its neighbour is also Δt. Therefore, the synchronism of the impulses on the entire TLM mesh is still ensured.

4.3 The Scattering Matrix at the Interface

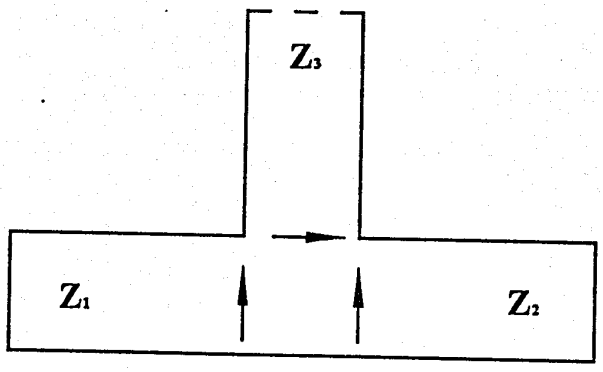

Fig 4.2: The junction of the series stub and the TLM mesh line

The scattering matrix at the interface can be obtained by analyzing the three-port network which consists of the stub and two transmission lines of the TLM mesh.

The normalized characteristic impedances of the link transmission lines are equal to 1. The normalized characteristic impedance of the stub will depend on the capacitance to be simulated. The relationship between them will be discussed later.

Assuming that the stub has a normalized characteristic impedance z_0, we have:

$$z_1 = 1 \tag{4.6}$$

$$z_2 = 1 \tag{4.7}$$

$$z_3 = z_0 \tag{4.8}$$

Using transmission line theory, the S-parameters of the three-port network in figure 4.2 can be calculated as below:

$$S_{11} = \frac{z_0}{z_0 + 2}$$
$$S_{22} = \frac{z_0}{z_0 + 2}$$
$$S_{33} = \frac{2 - z_0}{z_0 + 2} \quad .$$

Suppose a unit voltage impulse is incident on port 1, then the current at port 1 will be

$$i_1 = \frac{(1 - S_{11})}{z_1} = \frac{2}{z_0 + 2} \quad .$$

If there is no input from the other two ports, the currents at port 2 and port 3 will be

$$i_2 = \frac{S_{21}}{z_2} = S_{21}$$

$$i_3 = -\frac{S_{31}}{z_3} = -\frac{S_{31}}{z_0} \quad .$$

Because the node currents in this structure are identical, i.e.

$$i_1 = i_2 = i_3 \quad ,$$

then from the above equations, we can get:

$$S_{21} = \frac{2}{2 + z_0} \tag{4.9}$$
$$S_{31} = \frac{-2z_0}{2 + z_0} \quad . \tag{4.10}$$

In the same way, we can find the other S-parameters as

$$S_{12} = \frac{2}{2 + z_0} \tag{4.11}$$
$$S_{32} = \frac{2z_0}{2 + z_0} \tag{4.12}$$
$$S_{13} = \frac{-2}{2 + z_0} \tag{4.13}$$
$$S_{23} = \frac{2}{2 + z_0} \quad . \tag{4.14}$$

Assuming $z_r = 2 + z_0$, and combining equations (4.9)-(4.17), we get the scattering matrix as:

$$\begin{bmatrix} r_1 \\ r_2 \\ r_3 \end{bmatrix}_k = \frac{1}{z_r} \begin{bmatrix} z_0 & 2 & -2 \\ 2 & z_0 & 2 \\ -2z_0 & 2z_0 & 2 - z_0 \end{bmatrix} \cdot \begin{bmatrix} i_1 \\ i_2 \\ i_3 \end{bmatrix}_k$$

4.4 Simulation of a Series-Connected Constant Capacitance

In order to simulate the series-connected capacitance, we need to find out the relationship between z_0 of the stub and the capacitance to be simulated. As we know, the open-circuited stub is equivalent to a lumped capacitance (C_{ad}) at the other end in the relatively low frequency range ($\frac{\Delta l}{\lambda} \ll 1$):

$$C_{ad} = C \frac{1}{z_0} \frac{\Delta l}{2} \quad . \tag{4.15}$$

Here C is the capacitance per unit length of the TLM mesh lines.

Referring to equation (2.21) which says that $C = \epsilon_0$, we get:

$$C_{ad} = \frac{\epsilon_0 \Delta l}{2 z_0} \tag{4.16}$$

where

Δl = The mesh parameter

ϵ_0= The dielectric permittivity of free space

z_0= The normalized characteristic impedance of the stubs.

Due to the factor of $\frac{1}{\sqrt{2}}$ in the transformations of frequency and impedance between the TLM mesh and the real circuit it simulates, to simulate a series capacitance C_s, the capacitance added to the TLM mesh C_{ad} should be:

$$C_{ad} = 2C_s \tag{4.17}$$

Hence, to simulate C_s, we need the characteristic stub impedance to be

$$z_0 = \frac{\epsilon_0 \triangle l}{4C_s} \quad . \tag{4.18}$$

As an example, we simulate a simple resonator with a series capacitance at the centre (shown in Figure 4.3); the corresponding TLM mesh is shown in figure 4.4.

Simulation is done by the algorithm developed in the previous sections and equation (4.18); the different resonant frequencies (f_s) corresponding to the different series capacitances can be obtained from the TLM simulation followed by Fourier transformation.

For this simple case, the analytical solution of the resonant frequencies can be easily found. First, the analytical solution for the resonant frequency (f_0) of the resonator without series capacitance is:

$$f_0 = \frac{c}{2(20 \triangle l)} = 7.495(GHz) \tag{4.19}$$

With the series capacitance C_s, the first resonant frequency f_a must satisfy:

$$-\frac{1}{2\pi f_a C_s} = 2Z_t cot(\frac{\pi f_a}{2f_0}) \tag{4.20}$$

where

$$Z_t = \frac{\eta_0}{\sqrt{\epsilon_r}} \tag{4.21}$$

By solving the above equation, values of f_a corresponding to different C_s are obtained and listed in table 4.1. Comparing the analytical and simulation results in table 4.1, we find they agree very well over a wide range of C_s.

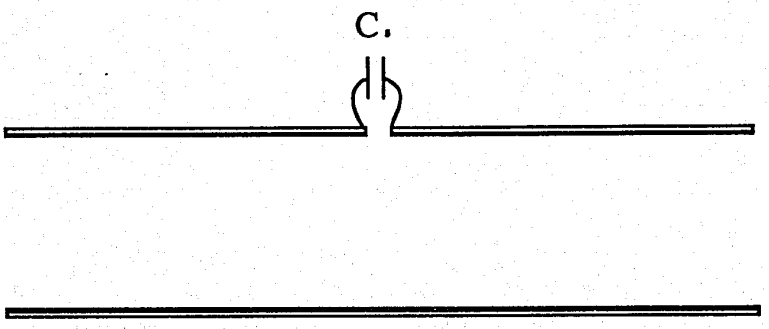

Fig. 4.3: A resonator with a series capacitance at its centre.

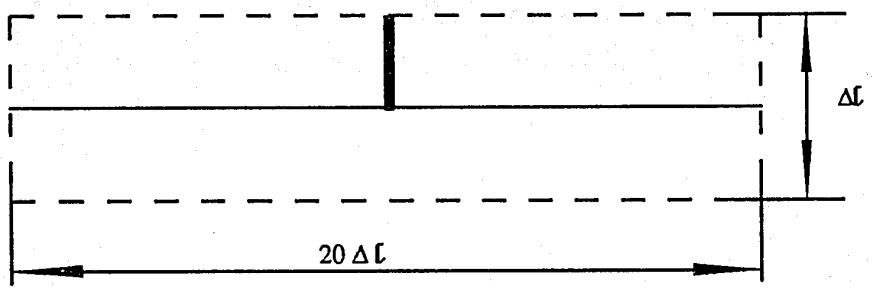

Fig. 4.4 : The TLM mesh for figure 4.3 . A series stub is inserted at the centre.
$\Delta\ell = 1$ mm.

Magnetic wall

Open-circuited stub

$C_s(Pf)$	$f_s(GHz)$	$f_a(GHz)$	$Error = \frac{\lvert f_s - f_a \rvert}{f_a}(\%)$
0.001	14.640	14.659	0.1
0.01	12.596	12.448	1.2
0.05	9.587	9.492	1.0
0.1	8.540	8.639	1.1
0.5	7.814	7.755	0.8
2.0	7.593	7.561	0.7
4.0	7.545	7.528	0.2
6.0	7.529	7.517	0.2
8.0	7.520	7.512	0.1
10.0	7.515	7.508	0.09
12.0	7.512	7.506	0.08
14.0	7.510	7.504	0.08
20.0	7.504	7.501	0.04

Table 4.1 The simulation and analytical results for the first resonant frequency of the resonator in Fig. 4.3

4.5 Simulation of a Series-Connected Varactor Diode in a Microstrip Circuit

When the varactor diode is connected in series with a transmission line, it can be simulated by a series-connected stub which has variable characteristic impedance. The details are shown below.

Referring to figure 4.1, if the varactor diode is represented by the stub, with the assumption that the cathode of the diode is at x and the anode is at x+1, the voltage across the diode will be:

$$v = V_{bias} + V_{cathode} - V_{anode} \quad . \tag{4.22}$$

Here,

$$V_{cathode} = E(x)h \tag{4.23}$$

$$V_{anode} = E(x+1)h \tag{4.24}$$

where

h is the height of the substrate.

E is electric field intensity which can be obtained from equation (1.16).

When the voltage on the varactor diode is known, the capacitance of the varactor diode $C(v)$ can be found from equation (3.1) or other formulas provided.

By the equation (4.18), the capacitance is represented by a stub of characteristic impedance z_0:

$$z_0 = \frac{\epsilon_0 \triangle l}{4C(v)} \quad . \tag{4.25}$$

The varactor diode is simulated in the time domain by updating the characteristic impedance of the stub according to the voltage across the stub at the previous iteration. r_3 should be modified in the same way as in the section 3.2 in order to conserve the energy.

4.6 Simulation of a Series-Connected Varactor Diode Multiplier

In reference [7], a monolithic frequency doubler using a series-connected varactor diode is presented. The circuit details and the curve of the total capacitance of two series-connected varactor diodes vs. reverse bias voltage are given below.

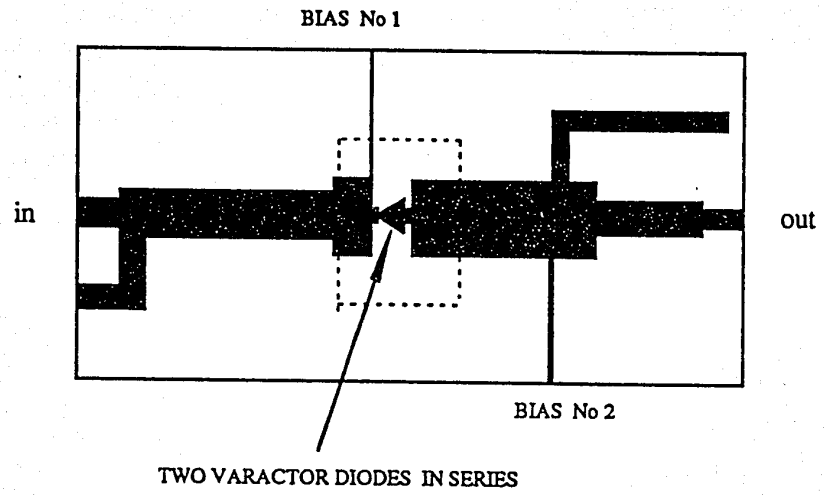

Fig. 4.5: Monolithic frequency doubler. Varactor diodes are integrated with microstripline circuits and bias lines. Dimensions of the chip are 4mm x 8mm.

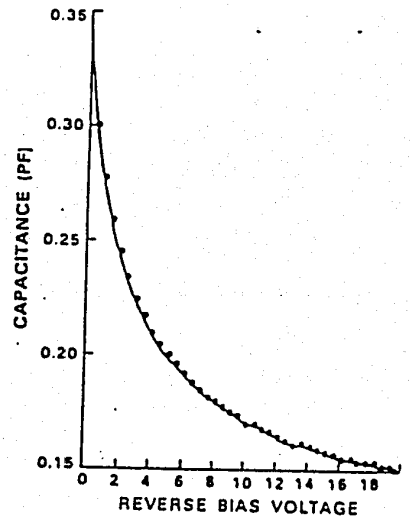

Fig.4.6 The junction capacitance vs reverse bias voltage of two K-band varactor diodes in series.

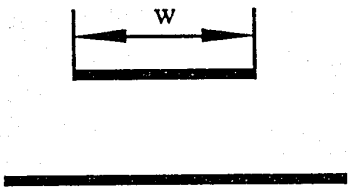

(a) The accurate model of microstrip in an homogeneous medium

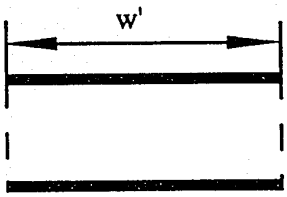

(b) The parallel-plate transmission line with perfect magnetic sidewalls on sides

Fig. 4.7 : Model for the microstrip with fringing effect

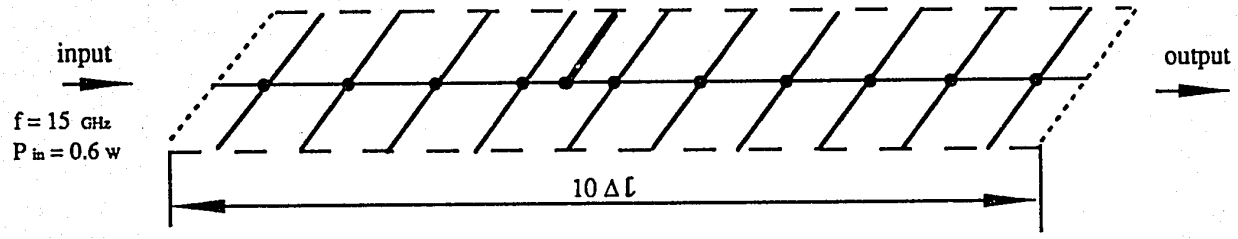

Fig. 4.8: The simulation mesh for the microstrip multiplier. $\Delta \ell$=0.05 mm

_ _ _ _ Magnetic wall

..... Absorbing boundary

▬▬▬ Open-circuited stub

For the convenience of computer programming, the voltage-dependent capacitance can be approximated by a fifth-order polynomial function.

$$C(v) = c[0] + c[1]v + c[2]v^2 + c[3]v^3 + c[4]v^4 + c[5]v^5 \tag{4.26}$$

The coefficients are:

$$\begin{aligned} c[0] &= 0.34751540 \\ c[1] &= 0.15259449 \\ c[2] &= 0.05335557 \\ c[3] &= 0.00984050 \\ c[4] &= 0.00088274 \\ c[5] &= 0.00003021 \end{aligned}$$

For the sake of simplicity, only the part of the circuit that is enclosed by the dashed line will be simulated. To model the microstrip circuit by the TLM mesh, two steps must be taken.

1. **Get the accurate model from the physical data of the microstrip**

   The accurate model of the single microstrip line is based on an equation for the impedance of microstrip in a homogeneous medium, z_0, and an equation for the microstrip effective dielectric constant, ϵ_ϵ[9].

   The impedance z_0 for the accurate model is:

$$z_0 = \frac{\eta}{2} ln[\ \frac{f(u)}{u} + \sqrt{1 + (\frac{2}{u})^2}\ ] \tag{4.27}$$

   where

$$f(u) = 6 + (2\pi - 6)exp[-(\frac{30.666}{u})^{0.7528}] \tag{4.28}$$

$$u = \frac{w}{h} \tag{4.29}$$

$$\eta = \frac{120\pi}{\sqrt{\epsilon_r}} \tag{4.30}$$

The effective dielectric constant ϵ_e is:

$$\epsilon_e(u, \epsilon_r) = \frac{\epsilon_r + 1}{2} + \frac{\epsilon_r - 1}{2}(1 + \frac{10}{u})^{-a(u)b(\epsilon_r)} \tag{4.31}$$

where

$$a(u) = 1 + \frac{1}{49} ln \frac{u^4 + (\frac{u}{52})^2}{u^4 + 0.432} + \frac{1}{18.7} ln[1 + (\frac{u}{18.1})^3] \tag{4.32}$$

$$b(\epsilon_r) = 0.564(\frac{\epsilon_r - 0.9)}{\epsilon_r + 3})^{0.053} \quad . \tag{4.33}$$

The dimensions of the microstrip to be simulated are:

$$\begin{aligned} w &= 0.8\, mm \\ h &= 0.175\, mm \\ \epsilon_r &= 13 \quad . \end{aligned}$$

Using the above equations, the accurate model will have:

$$\begin{aligned} z_o &= 14.6\, \Omega \\ \epsilon_e &= 10.15 \quad . \end{aligned}$$

2. **Represent the accurate model of the microstrip by a TLM mesh**

   By the first step, the accurate model has been established as in figure 4.7(a). To simulate it by the 2D-TLM method, it is necessary to represent it by a structure as shown in figure 4.7(b). This is known as the parallel plate model with magnetic side walls. The compensation of the fringing effect in (a) can be made by increasing the w to w' while ϵ_e, z_o and h will be the same for (a) and (b).

   For any transmission line, we have:

$$z_o = \frac{\sqrt{\epsilon_e}}{c\, C} \tag{4.34}$$

   For the structure in figure 4.7(b),

$$C = \frac{\epsilon_0 \epsilon_e w'}{h} \quad . \tag{4.35}$$

Combining equations (4.34) and (4.35), the expression for w' can be obtained:

$$w' = \frac{h}{z_0 c \epsilon_0 \sqrt{\epsilon_e}} \quad . \tag{4.36}$$

For this case, using equation (4.36)

$$w' = 1.44\, mm \tag{4.37}$$

Considering the operating frequency range of the multiplier, the parameter of the TLM mesh Δl is chosen as $0.05\, mm$. Discretizing the dimensions in figure 4.7(b), the TLM mesh for the multiplier is set up as in figure 4.8. The simulation gives the approximately 10 percent power efficiency (as shown in figure 4.9).

This result is not accurate enough to compare with the measurement data because several factors have not been considered in the series-connected stub. These factors such as the voltage-dependent resistance of the varactor diode, the parasitic parameters due to the package and link and the physical dimensions of the varactor diode will not be negligible at microwave frequency. Hopfully, the structure (as shown in figure 4.1) has the potential to simulate a contact impedance by adding an loss stub at the junction and to compensate the physical dimensions of the varactor diode by having the single open-circuited stub replaced by several open-circuited stubs in series. Further improvement for this model is certainly essential for accurate simulation of a real varactor diode.

In figure 4.9. the existence of sidelobes around the fundamental and the harmonics is due to the finite duration of the time domain impulse response. The Fourier transform of a finite duration impulse sequence is not a line spectrum but rather a superposition of (sin x)/x functions (Gibbs's phenomenon). This sidelobes may slightly shift the peaks and bring in the so called truncation error [11]. Increasing the number of iterations will narrow the sidelobes and thus decrease the truncation error.

4.7 Conclusion

In this chapter, a series capacitances has been successfully simulated by the a series-connected stub in a TLM mesh. This technique also can be used for the simulation of voltage-dependent capacitance. To accurately simulate a series varactor diode, this technique still need to be improved.

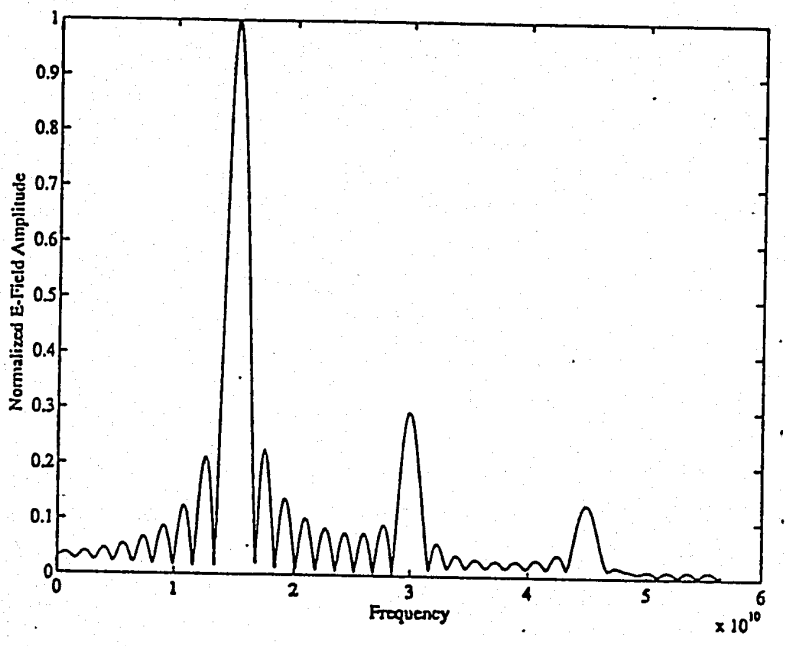

Fig 4.9: Frequency domain response for the mesh shown in figure 4.8

Chapter 5

Simulation of Voltage-Dependent Capacitance in Three Dimensions

5.1 Introduction

In this chapter, the simulation of a varactor diode is extended to a three-dimensional TLM mesh.

5.2 The TLM Three-Dimensional Expanded-Node

Reference [11] describes both shunt nodes and series nodes used in a two-dimensional TLM mesh. If the voltage on the shunt node represents an E-field in the medium, and the current in the series node represents an H-field in the medium, the following connection between the E- and H- fields can be developed for the shunt and series nodes in the x-z plane.

For the shunt node in the x-z plane we have:

$$\begin{aligned} \frac{\partial E_y}{\partial z} &= \mu \frac{\partial H_x}{\partial t} \\ \frac{\partial E_y}{\partial x} &= -\mu \frac{\partial H_z}{\partial t} \\ \frac{\partial H_x}{\partial z} - \frac{\partial H_z}{\partial x} &= -\epsilon \frac{\partial E_y}{\partial t} \end{aligned} \tag{5.1}$$

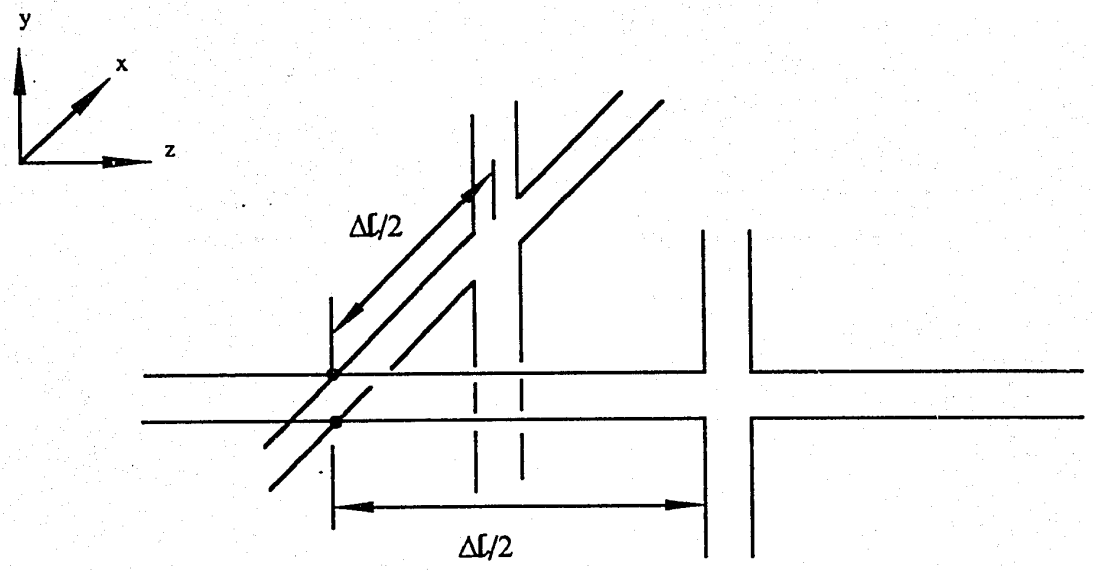

(a)

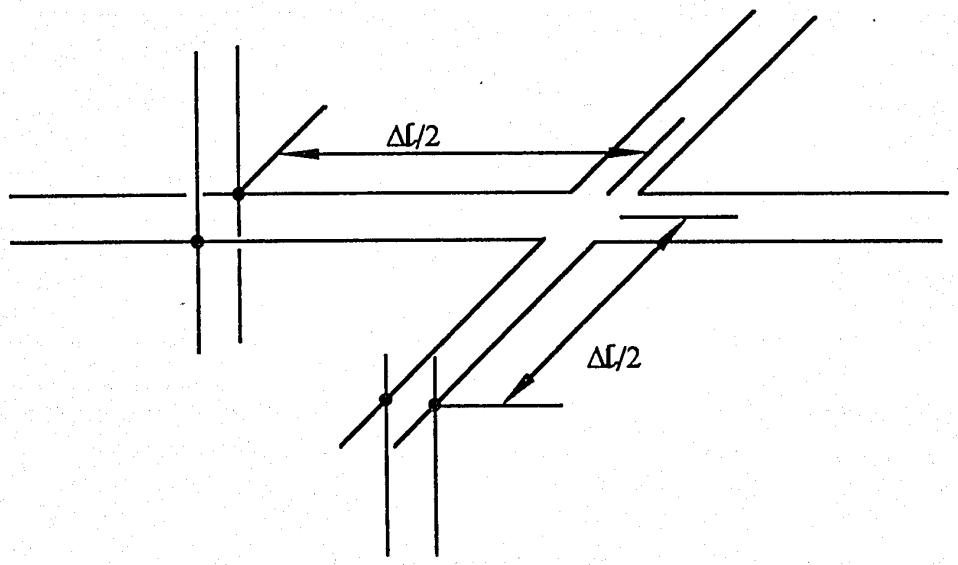

(b)

Fig. 5.1: (a) Part of a three-dimensional node containing one shunt and two series nodes
(b) Part of a three-dimensional node containing one series and two shunt nodes

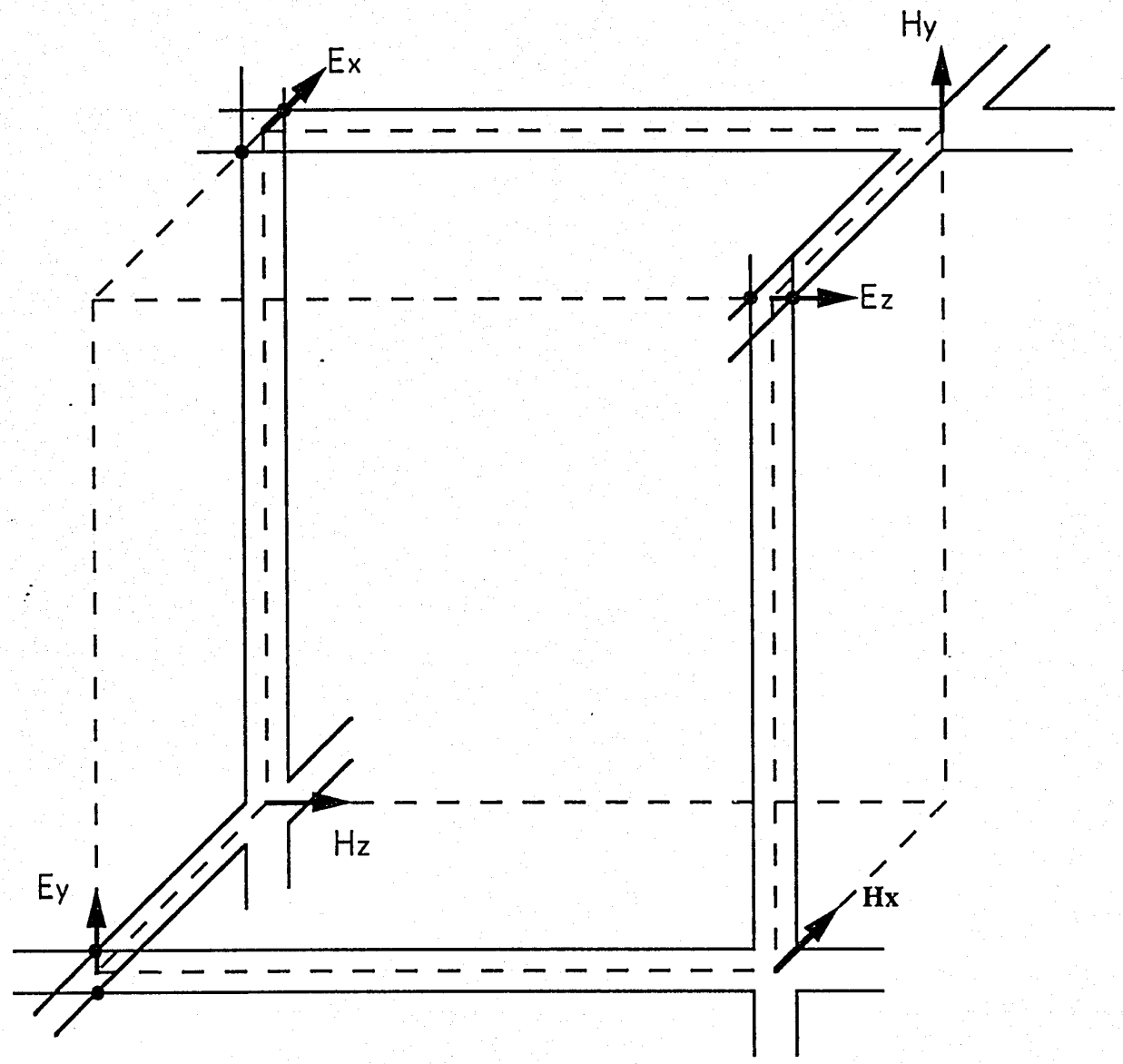

Fig. 5.2: Three-dimensional expanded TLM node

For the series node in the x-z plane, we have:

$$\begin{aligned} \frac{\partial H_y}{\partial x} &= \epsilon \frac{\partial E_z}{\partial t} \\ -\frac{\partial H_y}{\partial z} &= -\epsilon \frac{\partial E_x}{\partial t} \\ \frac{\partial E_x}{\partial z} - \frac{\partial E_z}{\partial x} &= -\mu \frac{\partial H_y}{\partial t} \end{aligned} \tag{5.2}$$

Considering a shunt node in the x-z plane connected to a series node in the y-z plane and a series node in the X-Y plane, as shown in Figure 5.1(a), we have:

$$\begin{aligned} \frac{\partial H_x}{\partial z} - \frac{\partial H_z}{\partial x} &= \epsilon \frac{\partial E_y}{\partial t} \\ \frac{\partial E_z}{\partial y} - \frac{\partial E_y}{\partial z} &= -\mu \frac{\partial H_x}{\partial t} \\ \frac{\partial E_y}{\partial x} - \frac{\partial E_x}{\partial y} &= -\mu \frac{\partial H_z}{\partial t} \end{aligned} \tag{5.3}$$

Considering a series node in the x-z plane connected to a shunt node in the y-z plane and a shunt node in the X-Y plane, as shown in Figure 5.1(b), we have:

$$\begin{aligned} \frac{\partial E_x}{\partial z} - \frac{\partial E_z}{\partial x} &= -\mu \frac{\partial H_y}{\partial t} \\ \frac{\partial H_z}{\partial y} - \frac{\partial H_y}{\partial z} &= \epsilon \frac{\partial E_x}{\partial t} \\ \frac{\partial H_y}{\partial z} - \frac{\partial H_x}{\partial y} &= \epsilon \frac{\partial E_z}{\partial t} \end{aligned} \tag{5.4}$$

Equations (5.3) and (5.4) together complete the description of the three-dimensional Maxwell's equations. So, the basic unit of a network (i.e. the expanded node) which supports the expansions of the three-dimensional Maxwell's equations can be built up by connecting the circuit of Figure 5.1(a) and the circuit of Figure 5.1(b). The three-dimensional TLM network model is shown both in Figure 5.2 and Figure 5.3. This three-dimensional TLM mesh has alternate shunt and series nodes in any of the co-ordinate directions. As shown in Figure 5.2, the three E-field components are represented by the voltages on the shunt nodes, and the three H-field components are represented by the currents on the series nodes. Since the six components of the electromagnetic field are

distributed among the corners of the node cube, this node is called the "expanded node". The transmission line which links the neighbour nodes has a length of $\frac{\Delta l}{2}$. Since there are two different kinds of nodes in the expanded node, one iteration includes separate steps of scattering and transmission. First the scattering happens on either the shunt or the series node, then the impulses travel and reach the other kind of node. The same process is repeated at every iteration. This model can also be used for inhomogeneous problems. To account for dielectric and magnetic mediua, open-circuited and short-circuited stubs are added to shunt and series nodes, respectively. To account for dielectric losses, stubs of infinite length can be added to the shunt nodes. When these features are included, the general expanded-node is as shown in Figure 5.4. The scattering matrices of the shunt and series nodes will be the same as in the two-dimensional cases. Since the shunt nodes double the capacitance (C) per unit length of the transmission line and the series nodes double the inductance (L) per unit length of the transmission line, if the free-space velocity c is given by:

$$c = \frac{1}{\sqrt{LC}} \quad , \tag{5.5}$$

then the low-frequency velocity of waves on the three-dimensional model v_n will be:

$$v_n = \frac{1}{\sqrt{2L2C}} = \frac{c}{2} \quad . \tag{5.6}$$

5.3 Simulation of the Varactor Diode in the Expanded-Node

Using the same idea as in the two-dimensional case, the model for a varactor diode which is connected in parallel to the microstrip circuit can be easily extended to the three-dimensional TLM mesh. As shown in figure 5.5, the varactor diode can be represented by a three-dimensional submesh. It is essential that the volume of the submesh equals the volume of the diode package.

The capacitance and the resistance of the submesh between the strip and the ground will be:

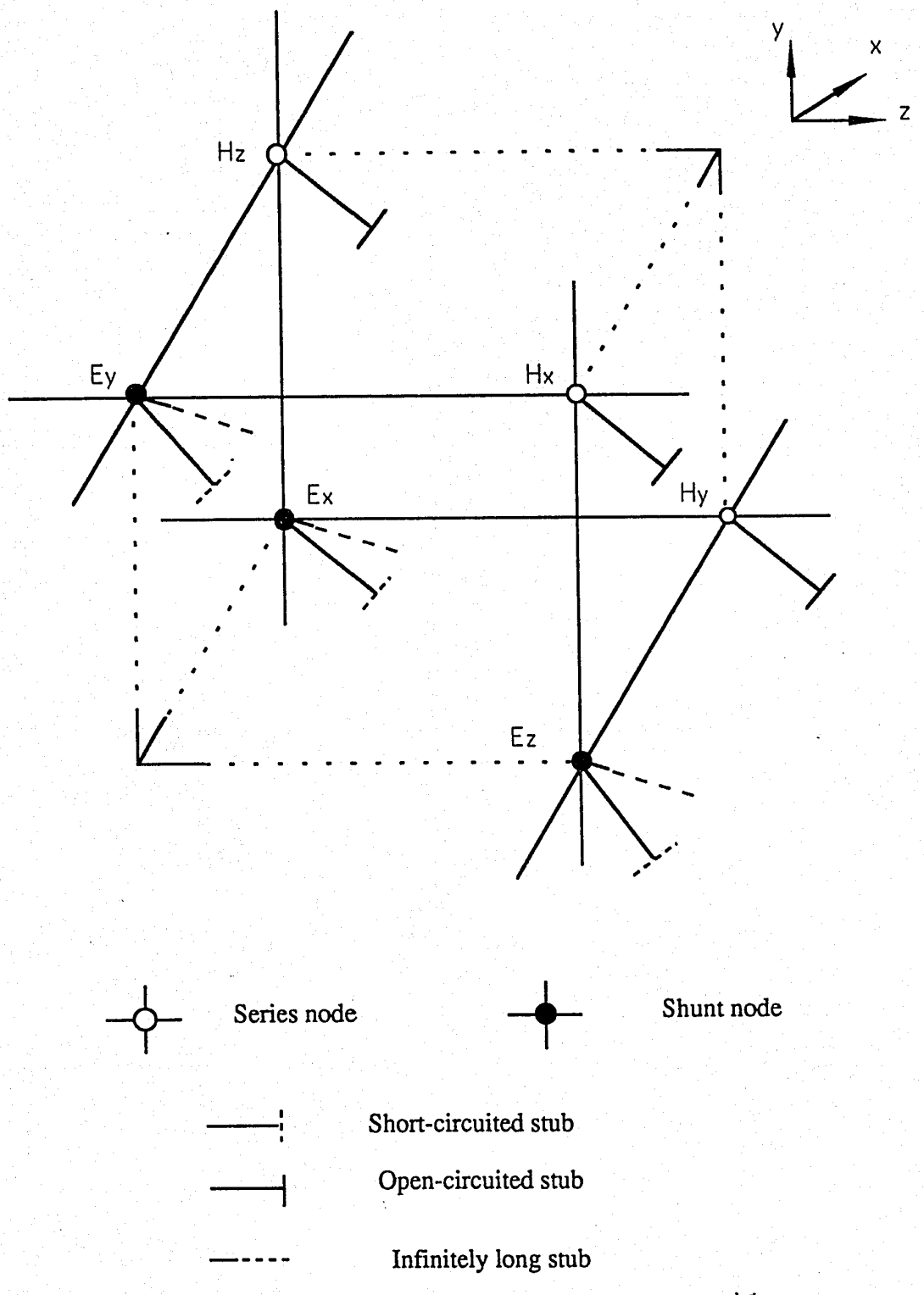

Fig. 5.3 : General expanded-node

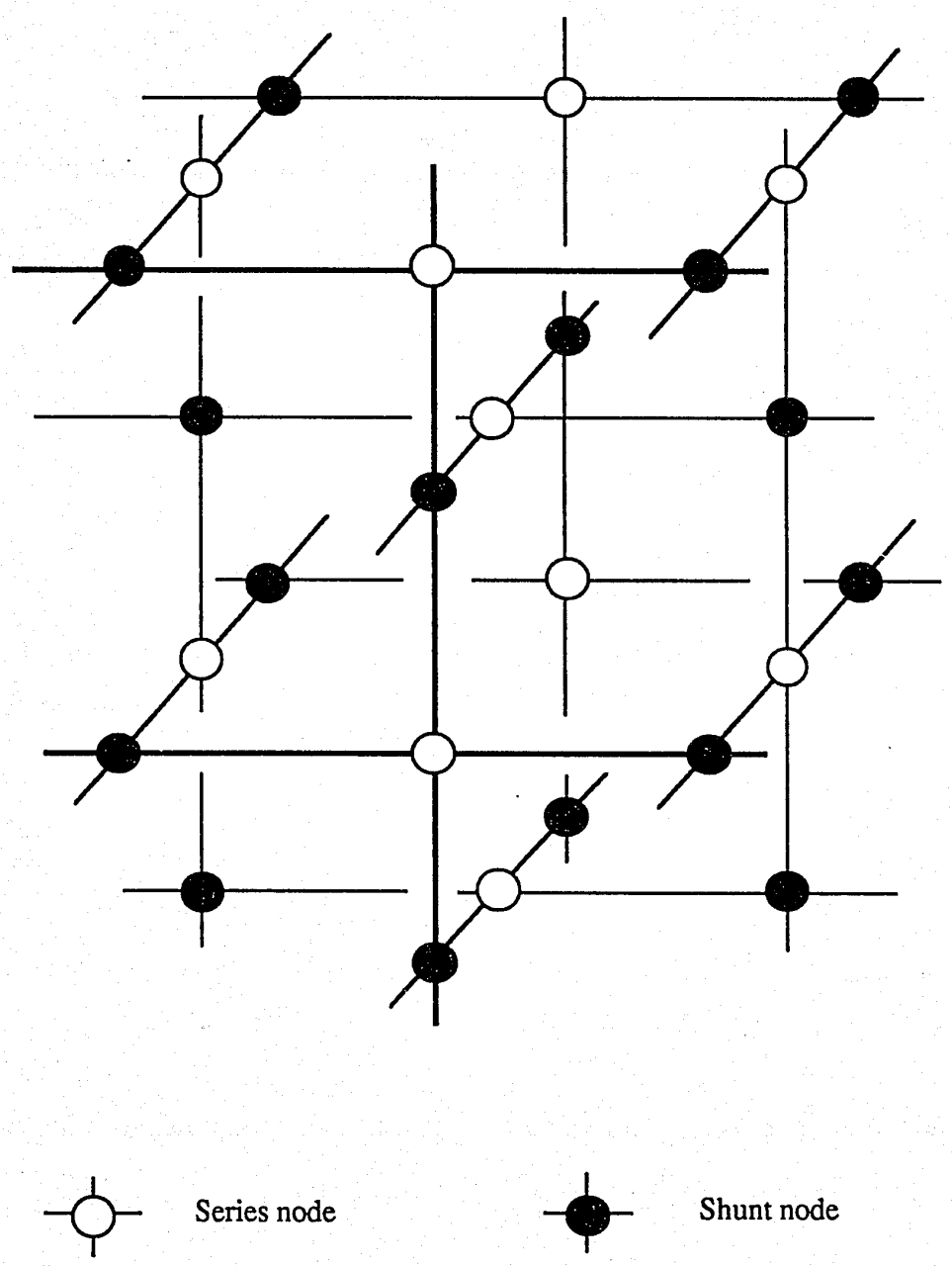

Fig. 5.4: Three-dimensional TLM mesh

$$C = \frac{\epsilon_0 \epsilon_r A}{h} \tag{5.7}$$

$$R = \frac{h}{A\sigma} \quad . \tag{5.8}$$

To make this capacitance and resistance equivalent to the effect of the varactor diode in the circuit, we compare the above equations with equations (3.8) and (3.9) and find that the variable permittivity and conductivity of the submesh will be:

$$\begin{aligned} \epsilon_r(v) &= \frac{h}{A\epsilon_0}\left[\frac{C_{j0}}{\sqrt{1-\frac{v}{\phi_0}}} + C_{dv}\right] \qquad \text{for} \quad v < \phi_0/2 \\ &= \frac{h}{A\epsilon_0}\left[\sqrt{2}C_{j0}(\frac{v}{\phi_0} + \frac{1}{2}) + C_{dv}\right] \quad \text{for} \quad v \geq \phi_0/2 \end{aligned} \tag{5.9}$$

$$\sigma(v) = \frac{h}{A}\frac{eI_s}{kT}\exp(\frac{ev}{kT}) \quad . \tag{5.10}$$

v is the voltage applied to the varactor between the anode and cathode. It can be calculated by:

$$v = E_y p \triangle l \tag{5.11}$$

$$E_y \equiv V_y \tag{5.12}$$

By updating the voltage-dependent characteristic admittance of the open-circuited stub (y_0) and the voltage-dependent conductivity of the loss stub (g_0) on the shunt node in the submesh for each interation, the varactor diode is simulated. As an example, a very simple 3D-TLM mesh as shown in figure 5.6, which involves a submesh for the varactor diode, is simulated with the above formulas. The simulation result (see figure 5.7) the frequency domain shows the frequency multiplication very clearly.

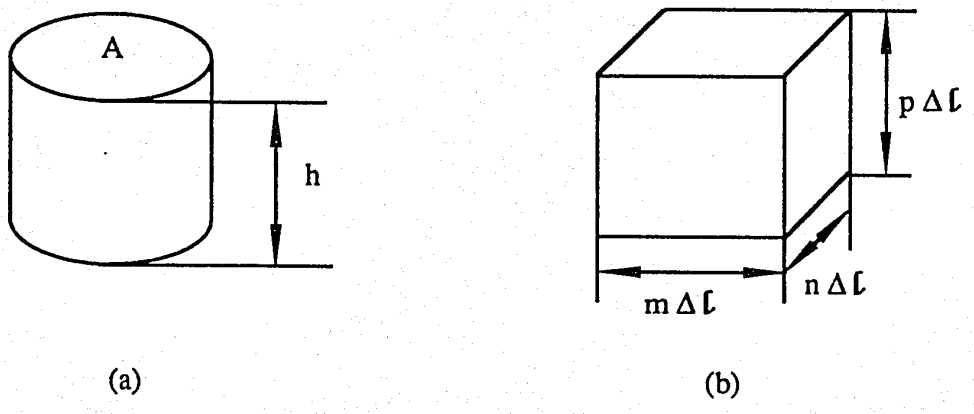

Fig. 5.5 : (a) The packaged varactor diode
(b) The three-dimensional submesh for the simulation of the diode

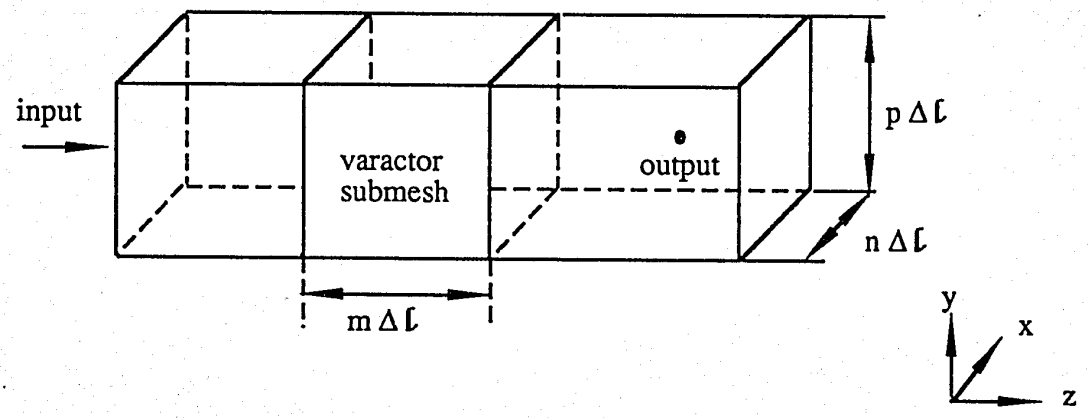

Fig. 5.6: The 3-D TLM mesh with a submesh for a varactor diode, $\Delta\ell$=0.5 mm.
m =5 n=8 p=3

The parameters of a Schotty barriers varactor diode are:
ϕ_o= 0.7 (v)
C_o=2.5 (pF)

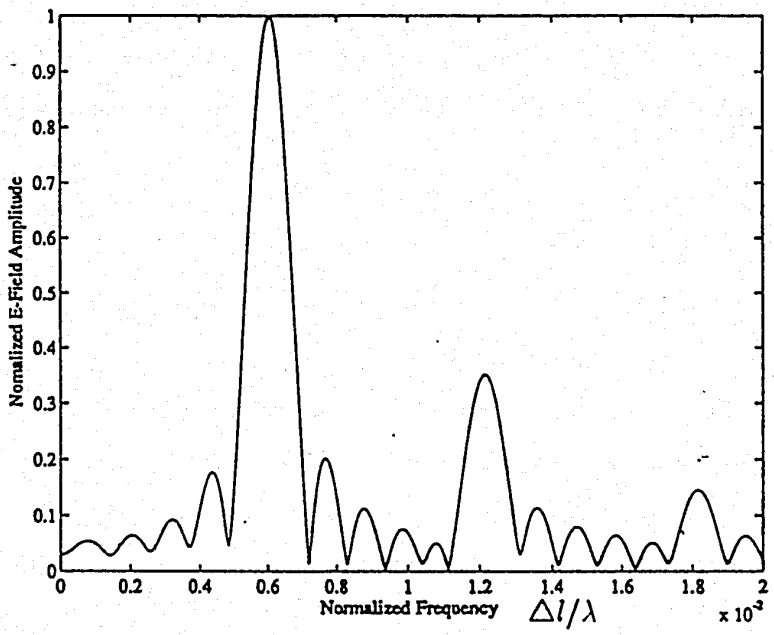

Fig 5.7: Frequency domain response for the mesh shown in figure 5.6

Conclusion

The new models developed in chapter 2 have been used to simulate both constant capacitance and voltage-dependent capacitance. At relatively low frequencies ($\frac{\Delta l}{\lambda} \ll 1$), the results agree well with the results obtained by other numerical methods or analytical solutions.

Both the open-circuited and the capacitance-loaded stub models have been used for the simulation of varactor diodes. The two models give similar simulation results. The open-circuited stub model has the advantages that it is unconditionally stable and less computationally demanding.

A new TLM structure, its scattering matrix and transmission formulas have been developed for simulating a series capacitance. Using this method, constant capacitance can be simulated accurately. Also, the principal portion of a varactor diode mutiplier has been modeled with this approach. In this case, data for a realistic circuit are used. The result obtained is quite reasonable. In this thesis, the discussion is limited to the lossless case. It is, however, possible to simulate a lossy series-connected varactor diode by introducing another lossy stub together with the open-circuited stub.

The simulation of varactor diodes has also been extended to the three-dimensional expanded-node. But it is still a challenging problem to simulate a real varactor diode due to the many parasitics.

Bibliography

[1] S. Akhtarzad, "Analysis of lossy microwave structures and microstrip resonators by the TLM method," Ph.D. Dissertation, University of Nottingham, England, July 1975.

[2] D. A.Al-Mukhtar and J.E. Sitch, "Transmission-line matrix method with irregularly graded space," *IEE Proc., Part H: Microwaves, Opt. Antennas,* vol. 128, pp. 299-305, Dec. 1981.

[3] S.Akhtarzad and P.B. Johns, "Numerical solution of lossy waveguides: T.L.M. computer program," *Electron. Lett.*, vol. 10, pp. 309-311, July 25, 1974.

[4] S.Akhtarzad and P.B. Johns, "Solution of 6-component electromagnetic fields in three space dimensions and time by the T.L.M. method," *Electron. Lett.*, vol. 10, pp. 535-537, Dec. 12, 1974.

[5] P. B. Johns and R. L. Beurle, "Numerical solution of two-dimensional scattering problems using a transmission-line matrix", *Proc. IEE.* Vol. 118, no. 9, pp. 1203-1208, Sept. 1971.

[6] P. B. Johns and M. O'Brien, "Use of the Transmission-line Modelling (TLM) method to solve nonlinear lumped networks", *Radio Electron. Eng.*, Vol. 50, pp. 59-70, 1980.

[7] A. Chu, W.E. Courtney, L. J. Mahoney, R.W. McClelland and H. A. Atwater, "GaAs monolithic frequency doublers with series connected varactor diodes", *Microwave and Millimeter-Wave Monolithic Circuits Symposium Digest* pp. 74-77, May 1984.

[8] I. Getreu, "Modelling the Bipolar Transistor, Part II", Electronics, pp. 71-75, Oct.31,1974.

[9] E. Hammerstad and Jensen, "Accurate models for microstrip computer-aided design", ELAB, 7034 Trondheim-NTH, Norway.

[10] W. J. R. Hoefer, "The transmission line matrix method – theory and applications", *IEEE Trans. Microwave Theory and Techniques*, Vol. MTT-33, no. 10 pp. 882-893, Oct. 1985.

[11] "The transmission line matrix (TLM) method", in *Numerical Techniques for Microwave and Millimeter Wave Passive Structures.* Chapter 8, T. Itoh, Ed. New York: John Wiley, 1989, pp. 496-591.

[12] P.B. Johns, "The general 2-D shunt node waveguide problems using a transmission-line matrix," *IEEE Trans. Microwave Theory Techniques*, vol. MTT-22, pp. 1086-1091, Aug. 1972.

[13] P.B. Johns. "The solution of inhomogeneous waveguide problems using a transmission-line matrix," *IEEE Trans. Microwave Theory Tech.*, vol MTT-22, pp. 209-215, Mar. 1974.

[14] S.A. Kosmopoulos , W.J.R. Hoefer and A. Gagnon, "Nonlinear TLM modelling of high-frequency varactor multiplier and halvers", *International Journal of Infrared and Millimeter Waves,* pp. 343-352,1989.

[15] G. Kron, "Equivalent circuit of the field equations of Maxwell–I," *Proc. IRE*, vol.32, pp.289-299, May 1944.

[16] L. A. Newcombe and J. E. Sitch, "Reactive nonlinearities in transmission-line models", *Proc. IEE A*, Vol. 132, pp. 95-98, 1985.

[17] A. V. Oppenheim and R. W. Schafer, "Transform Analysis of Linear Time-Invariant Systems" in *Discrete-Time Signal Processing*, Chapter 5, Prentice-Hall International, Inc. 1989.

[18] P. Penfield and R. P. Rafuse , "Varactor Applications", *The M.I.T. Press*, Massachusetts Institute of Technology, 1962.

[19] P. Russer, P. P. M. So, and W.J.R. Hoefer, "Modelling of Nonlinear Active Regions in TLM", *IEEE Microwave and Guided Wave Letters.* Vol. 1 no. 1, January 1991.

[20] W. J. R. Hoefer and P. P. M. So, *The Electromagnetic Wave Simulator.* Chapter 5, New York: John Wiley & Son Ltd. 1991.

[21] J.R. Whinnery and S. Ramo, "A new approach to the solution of high-frequency field problems," *Proc. IRE*, vol. 32, pp. 284-188, May 1944.